

การหาลักษณะเฉพาะเชิงโครงสร้างของฟิล์มทวิบิกเกลเลียมไนไตรด์ ด้วยกล้องจุลทรรศน์อิเล็กตรอน
ชนิดส่งผ่าน

นางสาวสุรางค์ สุนนาวดี

ศูนย์วิทยทรัพยากร

วิทยานิพนธ์นี้เป็นส่วนหนึ่งของการศึกษาตามหลักสูตรปริญญาวิทยาศาสตรมหาบัณฑิต
สาขาวิชาฟิสิกส์ ภาควิชาฟิสิกส์

คณะวิทยาศาสตร์ จุฬาลงกรณ์มหาวิทยาลัย

ปีการศึกษา 2553

ลิขสิทธิ์ของจุฬาลงกรณ์มหาวิทยาลัย

STRUCTURAL CHARACTERIZATION OF CUBIC GaN FILMS USING
TRANSMISSION ELECTRON MICROSCOPY



Miss Surang Sumnavadee

A Thesis Submitted in Partial Fulfillment of the Requirements
for the Degree of Master of Science Program in Physics

Department of Physics

Faculty of Science


Chulalongkorn University

Academic year 2010


Copyright of Chulalongkorn University

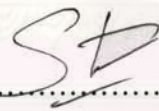
Thesis Title STRUCTURAL CHARACTERIZATION OF CUBIC GaN
FILMS USING TRANSMISSION ELECTRON MICROSCOPY
By Miss Surang Sumnavadee
Field of study Physics
Thesis Advisor Assistant Professor Sakuntam Sanorpim, Ph.D.
Thesis Co-advisor Assistant Professor Boonchoat Paosawatyanong, Ph.D.

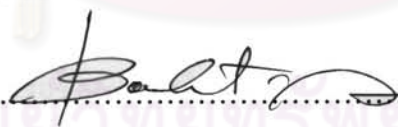
Accepted by the Faculty of Science, Chulalongkorn University in Partial
Fulfillment of the Requirements for the Master's Degree

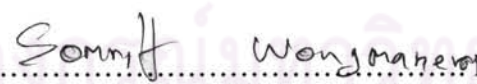

..... Dean of the Faculty of Science
(Professor Supot Hannongbua, Dr. rer. nat.)


THESIS COMMITTEE


..... Chairman
(Assistant Professor Patcha Chatraphorn, Ph.D.)


..... Thesis Advisor
(Assistant Professor Sakuntam Sanorpim, Ph.D.)


..... Thesis Co-advisor
(Assistant Professor Boonchoat Paosawatyanong, Ph.D.)


..... Examiner
(Somrit Wongmanerod, Ph.D.)


..... External Examiner
(Noppadon Nuntawong, Ph.D.)

สุรางค์ สุมนาวดี: การหาลักษณะเฉพาะเชิงโครงสร้างของฟิล์มคิวบิกแกเลียมไนไตรด์ ด้วยกล้องจุลทรรศน์อิเล็กตรอนชนิดส่งผ่าน (STRUCTURAL CHARACTERIZATION OF CUBIC GaN FILMS USING TRANSMISSION ELECTRON MICROSCOPY)

อ. ที่ปรึกษาวิทยานิพนธ์หลัก: ผศ.ดร.สฤทธธรรม เสนาะพิมพ์, อ. ที่ปรึกษาวิทยานิพนธ์ร่วม: ผศ.ดร.บุญโชติ เผ่าสวัสดิ์ขจรยง, 59 หน้า.

ฟิล์มคิวบิกแกเลียมไนไตรด์ (cubic GaN, c-GaN) ที่ปลูกผลึกด้วยวิธีเมทอลออร์แกนิกเวเปอร์เฟสเอพิแทกซีได้ถูกตรวจสอบด้วยกล้องจุลทรรศน์อิเล็กตรอนชนิดส่งผ่าน (Transmission Electron Microscope, TEM) เพื่อประเมินผลกระทบของเงื่อนไขการปลูกผลึกที่มีต่อคุณภาพผลึกของฟิล์มที่ปลูกได้ฟิล์ม c-GaN ที่ใช้ในการศึกษาครั้งนี้ได้ถูกปลูกผลึกลงบนซับสเตรต GaAs ที่มีผิวระนาบ (001) และ (311) โดยใช้อุณหภูมิที่ต่างกันในการปลูกผลึกชั้นบัฟเฟอร์ GaN คือในช่วง 550-600°C พบว่าฟิล์ม c-GaN ทั้งหมดมีโครงสร้างหลักแบบซิงค์แบลนหรือโครงสร้างผลึกแบบคิวบิก อย่างไรก็ตามสำหรับฟิล์มซึ่งปลูกในอุณหภูมิที่สูงกว่าจะพบการก่อเกิดโครงสร้างผลึกแบบเฮกซะโกนอลปนอยู่กับโครงสร้างคิวบิกโดยวางตัวอยู่บนระนาบ {111} ซึ่งเกี่ยวข้องกับสแตกกิงฟอลท์ (Stacking Faults, SFs) ที่เริ่มก่อเกิดจากสเตป (111) บนผิวซับสเตรต GaAs ระนาบ (001) เพื่อลดการเกิดโครงสร้างผลึกแบบเฮกซะโกนอลในฟิล์ม c-GaN อุณหภูมิการปลูกชั้นบัฟเฟอร์ GaN ถูกหาอุณหภูมิที่ดีที่สุดและอุณหภูมินี้ส่งผลถึงการก่อเกิด SFs ในชั้นฟิล์ม c-GaN คุณภาพที่ดีที่สุดของฟิล์ม c-GaN ที่ถูกปลูกผลึกลงบนซับสเตรต GaAs ที่มีผิวระนาบ (001) ซึ่งให้ความบริสุทธิ์ของโครงสร้างผลึกแบบคิวบิก ได้รับโดยการปลูกด้วยอุณหภูมิการปลูกฟิล์ม GaN ที่ดีที่สุด 900°C และอุณหภูมิการปลูกบัฟเฟอร์อย่างต่ำที่ 575°C นอกจากนี้ฟิล์ม c-GaN ที่ถูกปลูกผลึกลงบนซับสเตรต GaAs ที่มีผิวระนาบ (311) ด้วยเงื่อนไขการปลูกเดียวกันแสดงให้เห็นการปรากฏของ SFs แต่โครงสร้างผลึกแบบเฮกซะโกนอลไม่ปรากฏให้เห็น จากผลทั้งหมดนี้แสดงให้เห็นว่า ฟิล์ม c-GaN ที่ถูกปลูกผลึกลงบนซับสเตรต GaAs ที่มีผิวระนาบ (311) แสดงถึงคุณภาพของฟิล์มที่ดีขึ้นด้วยความหนาแน่นของ SFs น้อยลงเมื่อเทียบกับฟิล์ม c-GaN ที่ถูกปลูกผลึกลงบนซับสเตรต GaAs ที่มีผิวระนาบ (001) ซึ่งอาจเกิดเนื่องจากความยากของการเกิดสเตป (111) บนผิวซับสเตรต GaAs ระนาบ (311) ที่ใช้ในการปลูก

ภาควิชาฟิสิกส์.....
สาขาวิชา.....ฟิสิกส์.....
ปีการศึกษา2553.....

ลายมือชื่อนิสิต..... สุรางค์ สุมนาวดี.....
ลายมือชื่อ.ที่ปรึกษาวิทยานิพนธ์หลัก..... SF.....
ลายมือชื่อ.ที่ปรึกษาวิทยานิพนธ์ร่วม.....

5072534023: MAJOR PHYSICS

KEYWORDS: TRANSMISSION ELECTRON MICROSCOPY / CUBIC GaN /
STRUCTURAL PROPERTY / METALORGANIC VAPOUR PHASE EPITAXY

SURANG SUMNAVADEE: STRUCTURAL CHARACTERIZATION OF
CUBIC GaN FILMS USING TRANSMISSION ELECTRON MICROSCOPY.


ADVISOR: ASST. PROF. SAKUNTAM SANORPIM, Ph.D., CO-ADISOR:
ASST. PROF. BOONCHOAT PAOSAWATYANYONG, Ph.D., 59 pp.


Cubic GaN (c-GaN) films grown by metalorganic vapor phase epitaxy were investigated using transmission electron microscopy (TEM) to verify effects of growth conditions on the film quality. The c-GaN films used in this study were grown on GaAs (001) and (311) oriented substrates with different growth temperatures of the GaN buffer layers (550-600°C). It is found that all the c-GaN grown films have a cubic structure as a main crystal structure. However, for higher growth temperature, hexagonal phase inclusions found to easily construct along the {111} facets of c-GaN associated with the formation of stacking faults (SFs) starting from the (111) step on the GaAs (001) grown surface. To reduce a generation of hexagonal phase in c-GaN films, growth temperature of a GaN buffer layer is optimized and affected on the formation of SFs in the c-GaN films. The best quality of c-GaN films grown on GaAs (001) substrates with cubic phase purity was achieved by the growth with the optimum growth temperature of GaN films of 900°C and low buffer growth temperature of 575°C. Besides, the c-GaN film on GaAs (311) substrate with identical growth conditions results in the presence of SFs but the hexagonal single crystal is invisible. These results demonstrate that c-GaN on GaAs (311) exhibits a better film quality with lower density of SFs compared to that in c-GaN on GaAs (001). This might be due to a difficulty of a generation of the (111) step on the GaAs (311) grown surface.


Department:Physics.....

Field of study:Physics.....

Academic Year:2010.....

Student's Signature.....

Advisor's Signature.....

Co-advisor's Signature.....

Acknowledgements

I would like to express my deeply gratitude to my advisor, Assistant Professor Dr. Sakuntam Sanorpim, for the support, the precious advice and the knowledge all through these three years of my research. Also he has been giving the opportunity to present my work in many conferences and extended my thanks to my co-advisor, Assistant Professor Dr. Boonchoat Paosawatyanong.

I would like to thanks my thesis committee, Assistant Professor Dr. Patcha Chatraphorn, Dr. Somrit Wongmanerod and Dr. Noppadon Nuntawong for taking times from their busy schedules to be my thesis committee and giving me comments, suggestions, and useful additional information.

My special thanks goes to Professor Dr. Kentaro Onabe from the Onabe lab, Department of Advanced Materials Science, The University of Tokyo, Japan for providing the great GaN samples and extended to Visittapong Yodsri from TEM Lab, National Metal and Materials Technology Center (MTEC), Thailand for his TEM specimen preparation techniques.

I would like to acknowledge the financial supports from Graduate School Thesis Grant, Graduate School, Chulalongkorn University and from Conference Grant for Master Degree Student both of the Department of Physics, Faculty of Science and the Graduate School, Chulalongkorn University.

I would like to thanks all of my friends and all members of the Advanced Materials Physics Lab on the 19th floor of MHMK buildings for every joyful moment particularly, P'kwang and P'koi for giving me several helpful advice and discussion, Nick for his take care and cheer me up and the last one, I would like to heartfelt thanks my mom for everything.

Contents

	Page
Abstract (Thai)	iv
Abstract (English)	v
Acknowledgements	vi
Contents	vii
List of Tables	ix
List of Figures	x
 CHAPTER	
I Introduction	1
1.1 Overviews.....	1
1.2 Material problems.....	1
1.3 Objectives and organization of the thesis.....	4
II TEM and interpretation	6
2.1 TEM system.....	6
2.2 Interpretation of TEM results.....	10
2.2.1 Indexing diffraction spots.....	10
2.2.2 Diffraction-contrast imaging.....	14
III Experiments	16
3.1 MOVPE growth.....	16
3.2 Preparation of TEM specimen.....	18
3.2.1 Cross-section TEM specimen.....	19
3.2.2 Plan view TEM specimen.....	23
3.3 Optimization of polishing process.....	24
IV Microstructural Characterization of c-GaN on GaAs (001)	26
4.1 Sample Structure and Growth Conditions.....	26
4.2 Morphologies of Surface and Interface.....	28

	Page
4.3 Generation of defects in c-GaN with different growth temperature of GaN buffer layer.....	30
4.4 Growth conditions of c-GaN on GaAs with different growth temperature of film epilayer.....	37
4.5 Microstructural investigation of c-GaN on GaAs (001) substrate with different growth temperature of film epilayer.....	38
4.6 Summary.....	41
V Microstructural Characterization of c-GaN on GaAs (311).....	42
5.1 Sample Structure and Growth Conditions.....	42
5.2 Morphologies of Surface and Interface.....	43
5.3 Microstructures in c-GaN on GaAs (311).....	46
5.4 SFs in c-GaN on GaAs (311).....	48
5.5 Discussion.....	49
5.6 Summary.....	50
VI Conclusions.....	51
References.....	52
Appendix.....	55
Vitae.....	59

ศูนย์วิทยทรัพยากร
จุฬาลงกรณ์มหาวิทยาลัย

List of Tables

	Page
2.1 The comparison of electron sources; thermionic tungsten filament, thermionic Lanthanum Hexaboride (LaB_6) and field emission.....	8
2.2 The ratios of the reciprocal lattice spacing R_A/R_B	13



ศูนย์วิจัยทรัพยากร
จุฬาลงกรณ์มหาวิทยาลัย

List of Figures

	Page
1.1 Schematic illustrations of GaN crystal structures, (left-top) cubic structure, (right-top) hexagonal structure, (left-bottom) cubic structure along the [111] direction and (right-bottom) hexagonal structure along the [0001] direction. Note that the difference between these two crystal structures is only a rotation 60° along cubic [111] and hexagonal [0001] directions.....	2
1.2 Two dimensional Schematic illustrations of GaN crystal structure, (left) cubic structure along [110] direction and (right) hexagonal structure along [10-10] direction.....	3
1.3 Two dimensional Schematic illustrations of stacking fault; an insertion of one monolayer of hexagonal structure among cubic structures.....	3
2.1 The main features of a conventional transmission electron microscope.....	7
2.2 Schematic illustration of the incident electron beam and the diffracted electron beam in TEM [10]. R is a distance between the direct diffracted beams to the diffracted spots.....	10
2.3 Electron diffraction pattern obtained from c-GaN crystal along the [110] zone axis.....	11
2.4 Distance between the direct transmitted beam and diffraction spot A and spot B indicating as R_A and R_B , respectively.....	12
2.5 Streaking of reciprocal lattice points arising from precipitate plates lying parallel to the incident beam.....	14
3.1 The horizontal reactor of MOVPE system at the University of Tokyo, Japan; 2010.....	16
3.2 Sample model of c-GaN grown on GaAs (001) substrates with (left) different growth temperature 900, 930 and 960°C and (right) different growth temperature of nucleation layer 550, 575 and 600°C	17
3.3 The model 650 low speed diamond wheel saw.....	19
3.4 Sample model of the two pieces of specimen are stuck by M-BOND glue...	19

	Page
3.5 (left) The specimen is polished by the 9 μm diamond lapping film on the polisher, (right-top) Sample model of the clamped specimen is stuck on a triangular shaped glass and (right-below) showing the diamond grind size of diamond lapping films.	20
3.6 Precision Ion Polishing system (PIPs)	20
3.7 The surface of GaAs substrate surface, using as the specimen to optimize polishing process, without any polishing.....	22
3.8 Plan view SEM images showing the surfaces of specimens, which were polished by diamond-lapping films with different diamond grind sizes (0.5, 1, 3, 6 and 9 μm) and various speeds of the polisher (60, 100 and 130 rpm).	23
4.1 Schematic drawing of c-GaN sample grown on GaAs (001) substrate with different growth temperatures of LT-GaN buffer; 550, 575 and 600°C.....	26
4.2 SEM images showing a cross-section of the c-GaN films grown on GaAs (001) substrates with different growth temperatures of LT-GaN buffer; 550, 575 and 600°C.	27
4.3 TEM images showing plan-view micrographs and ED patterns of the c-GaN films grown with different growth temperature of GaN buffer layer; (a), (e) 550°C, (b), (f) 575°C and (c), (d), (g) 600°C.....	29
4.4 Cross-sectional TEM micrographs and ED patterns of c-GaN layers grown on GaAs (001) substrates with growth temperature of GaN buffer layer at 550°C.	31
4.5 Cross-sectional TEM micrographs and ED patterns of c-GaN layers grown on GaAs (001) substrates with growth temperature of GaN buffer layer at 550°C have taken at the GaN/ GaAs interface.....	31
4.6 Cross-sectional TEM micrographs and ED patterns of c-GaN layers grown on GaAs (001) substrates with growth temperature of GaN buffer layer at 575°C	32

	Page
4.7	Cross-sectional TEM (a) micrograph and (b), (c), (d) and (e) ED patterns of c-GaN layers grown on GaAs (001) substrates with growth temperature of GaN buffer layer at 600°C.....34
4.8	Cross-sectional TEM micrograph of c-GaN layers with growth temperature of GaN buffer layer at 600°C is highlighting at the V-shape voids which were caused by the As thermal decomposition.35
4.9	Dark-field (DF) images of c-GaN on GaAs substrates with different growth temperature of GaN buffer layer at (a) 550°C, (b) 575°C and (c) 600°C taken from the (1-100) of hexagonal diffraction spots near the (1-1-1) of cubic diffraction spots.....36
4.10	ED pattern of (b) cubic single crystal and hexagonal single crystal showing (a) the (1-100) of hexagonal diffraction spots near the (1-1-1) of cubic diffraction spots taken to form DF images in Fig. 4.9.....36
4.11	Sample model of c-GaN grown on GaAs (001) substrates with different growth temperature of films layer 900, 930 and 960°C.....37
4.12	Cross-sectional TEM micrographs and ED patterns of c-GaN layers grown on GaAs (001) substrates with growth temperature of films epilayer; (a), (d) 900°C, (b), (e) 930°C and (c), (f) 960°C with key-diagrams. The arrows indicate the positions of diffraction spots for the hexagonal phase single crystal.....38
4.13	(a) ED pattern of c-GaN layer grown at 960°C showing mixed cubic/hexagonal structure. The key-diagrams show diffraction patterns for hexagonal structures orientated along (b) [1-11] (open triangles) and (c) [-111] directions indicated as the open triangles parallelograms, respectively.....40
5.1	Schematic drawing of c-GaN sample grown on GaAs (311) substrate with growth temperature of c-GaN films layer 900°C and growth temperatures of LT-GaN buffer 575°C.....42

	Page
5.2 SEM images showing cross-section and surface of the c-GaN films grown on GaAs (311) substrate with growth temperature of c-GaN films layer 900°C and growth temperature of LT-GaN buffer layer 575°C.....	43
5.3 Showing plan-view micrographs and ED pattern of the c-GaN films grown GaAs (311) substrate.....	45
5.4 Cross-sectional TEM micrograph and ED pattern of c-GaN layers grown on GaAs (311) substrates with growth temperature of GaN films layer 900°C and growth temperature of LT-GaN buffer layer 575°C.....	47
5.5 Cross-sectional TEM (a) micrograph and (b) ED pattern of c-GaN films layer grown on GaAs (311) substrates with growth temperature of films layer 900°C and growth temperature of GaN buffer layer 575°C. Dark-field (DF) images of the diffracted spots have taken from (c) (311), (d) (1-11), (e) (-1-31) and (f) (-2-20).	48

CHAPTER I

INTRODUCTION

1.1 Overview

Group III-nitride semiconductors, including gallium nitride (GaN), indium nitride (InN) and aluminum nitride (AlN) have been received much attention and been investigated for many years as highly promising candidates for applications in opto-electronic and photovoltaic devices, giving the visible and ultra-violet emission operating at high temperature [1, 2, 3, 4] high breakdown voltage [5] and high pressure conditions [6]. Generally, these nitride semiconductors crystallize in Wurtzite (hexagonal) structure, which is thermodynamically stable phase and commercially available [7]. On the other hand, GaN is also crystallized in Zincblende (cubic) structure, which is metastable phase but has been intensively investigated [8, 9, 10]. It is due to the advantages of the cubic crystal compared to the hexagonal crystal. For instance, the cubic crystal is easier to be doped or alloyed, easier to be cleaved in the device processing and compatible with the GaAs-based devices. Besides, the cubic crystal has higher crystallographic symmetry, which results in superior electronic properties such as higher electron mobility, lower phonon scattering and lower electron effective mass. Therefore, the quality of cubic phase GaN (c-GaN) films have been improved and developed in various growth conditions [8, 11, 12].

1.2 Material problems

To control crystal structure, commonly, c-GaN films have to be grown on cubic substrates, such as gallium arsenide (GaAs) [13, 14, 15, 16, 17] and gallium phosphide (GaP) [18, 19, 20]. It was found that highly luminescent c-GaN films were grown on GaAs (001) substrates at relatively high growth temperature of 900°C [8, 9, 10]. However, GaAs substrate surface is very unstable at such high growth temperature (900°C), which is much higher than an As desorption temperature at ~615°C [21, 22]. This results in a formation of the (111)-steps, which relate to the formation of stacking faults (SFs), on the GaAs (001) surface. It is well known that correlation between c-GaN and hexagonal

phase GaN (h-GaN) exists along the $\langle 111 \rangle_{c\text{-GaN}}$ and $\langle 0001 \rangle_{h\text{-GaN}}$ crystal orientations. When c-GaN (111) plane is rotated 60° along the [111] direction, then the crystal structure of GaN is modified to be hexagonal structure with (0001) plane, as shown in Fig.1. As a result, both decomposition of As, which creates the (111)-steps on the GaAs (001) surface, and metastable phase of c-GaN have taken to immediate formation of hexagonal structure among the cubic structure. This results in formation of planar defects such as SFs (Fig. 1.3), twins and hexagonal phase inclusions which depend on the density of the hexagonal phase layers inserted in the c-GaN crystal along the (111) plane.

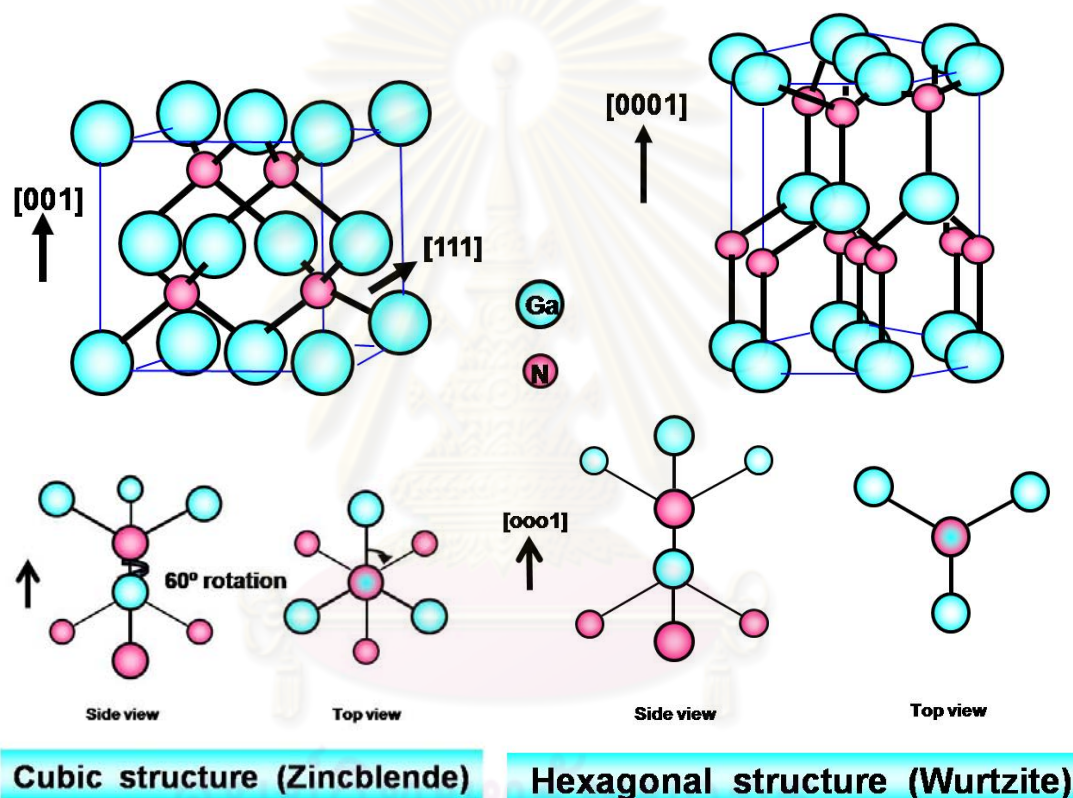


Figure 1.1: Schematic illustrations of GaN crystal structures, (left-top) cubic structure, (right-top) hexagonal structure, (left-bottom) cubic structure along the [111] direction and (right-bottom) hexagonal structure along the [0001] direction. Note that the difference between these two crystal structures is only a rotation 60° along cubic [111] and hexagonal [0001] directions.

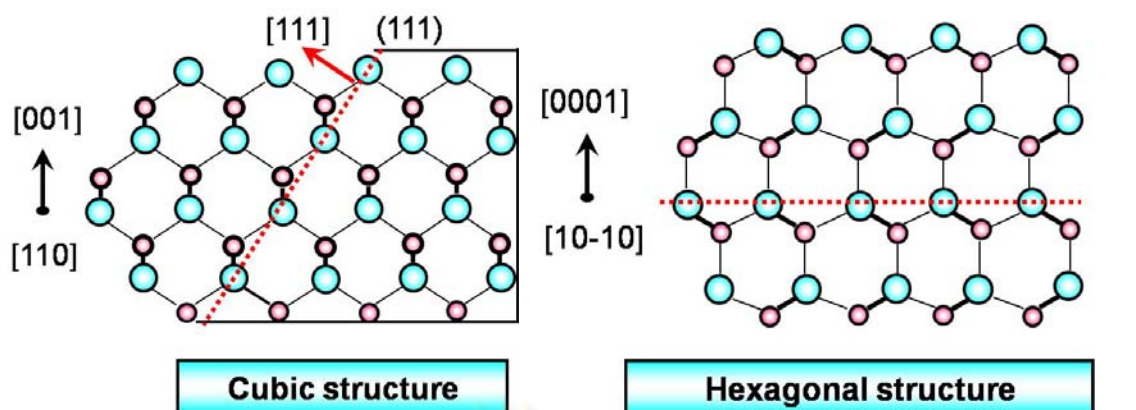


Figure 1.2: Two dimensional Schematic illustrations of GaN crystal structure, (left) cubic structure along $[110]$ direction and (right) hexagonal structure along $[10-10]$ direction

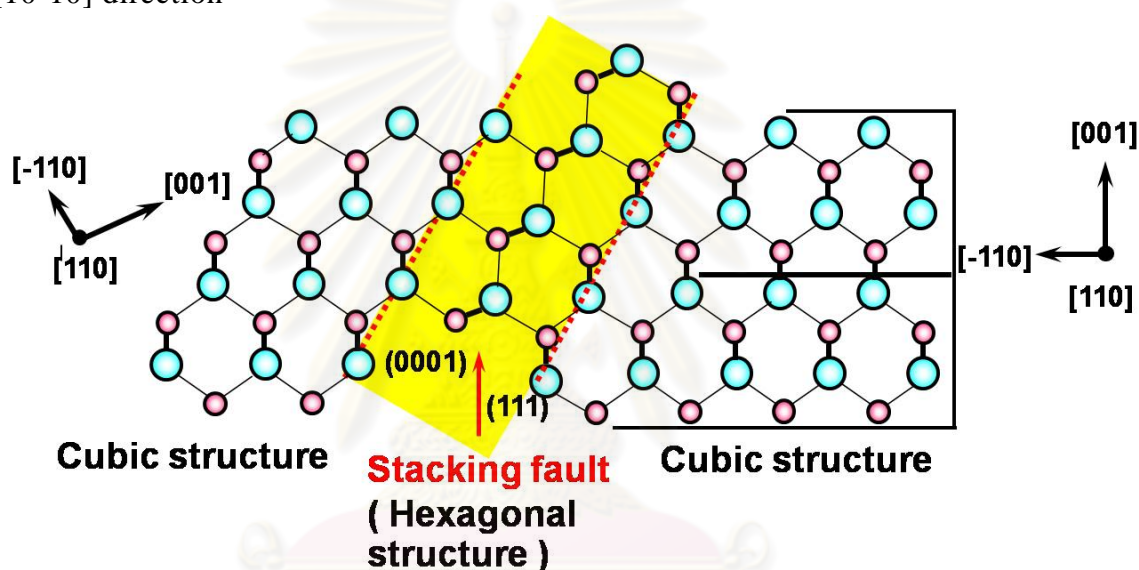


Figure 1.3: Two dimensional Schematic illustrations of stacking fault; an insertion of one monolayer of hexagonal structure among cubic structures

The planar defects can be classified by a number of hexagonal phase layers inserted in cubic structure along the (111) plane, such as

- (1) SFs; an insertion of one monolayer of hexagonal structure among cubic structures, which there are identical crystal orientations.
- (2) Twins; an insertion of a half monolayer of hexagonal structure among cubic structure, which are different crystal orientations.
- (3) Hexagonal phase sub-domain; the extension of SFs to be a single crystal of hexagonal structure.

Therefore, suitable cubic substrate and growth conditions are required to obtain c-GaN films with higher cubic phase purity. Sanorpim *et al.* [24] reported on a reduction of SFs and twins, which is likely resulted from their annihilation and termination within the c-GaN crystal due to the dominance of the lateral growth of the stable (311)A facets. This motivates us to investigate the structural characteristics of c-GaN film grown on the (311) oriented GaAs substrate. Since, it is expected to show a smoother surface and lower density of extended defects within the c-GaN grown film.

1.3 Objectives and organization of the thesis

The aim of the thesis is to investigate, analyze and assess the crystal quality of c-GaN films grown on GaAs (001) and GaAs (311) substrates by metalorganic vapor phase epitaxy (MOVPE). To understand the defect formation at the c-GaN/GaAs (001) interface, the c-GaN films grown with different growth temperatures of GaN buffer layer were selected. The focus is on the microstructures of c-GaN films analyzed using transmission electron microscopy (TEM); Electron Diffraction (ED), Bright-Field (BF) and Dark-Field (DF) images. To compare with the c-GaN films grown on GaAs (001) surface, microstructures of c-GaN film on GaAs (311) substrate also investigated by TEM. The goal is to find the optimum growth condition to grow pure c-GaN.

The thesis is organized as follows

Chapter 2 reviews principle of transmission electron microscopy, including advantages, limitation and interpretation of TEM results. In addition, preparation of thin film semiconducting specimen for TEM measurement is described.

Chapter 3 gives a growth procedure and growth conditions of c-GaN samples used in this work. Besides, optimization of the polishing process for preparation of cross-sectional specimen is demonstrated.

Chapter 4 focuses on the results investigated by TEM. We interpret the results obtained from ED patterns, BF and DF images and higher resolution BF-TEM images. Surface and interface morphologies of c-GaN/GaAs (001) primary

investigated by cross-sectional scanning electron microscopy (SEM) are described. Then, a deep insight in the micro-structural analysis using TEM is described in term of the growth temperature of GaN buffer layer. Finally, the film quality of c-GaN on GaAs (001) substrate is provided.

Chapter 5 focuses on the c-GaN films grown on the GaAs (311) substrate with the optimum growth conditions of c-GaN on GaAs (001). Microstructures of the films investigated by SEM and TEM are demonstrated and discussed in details. Then, we try to verify the reason for defect formation in c-GaN crystal based on the investigational results gained from c-GaN films grown on both the (001) and (311) substrate surfaces.

Finally, **Chapter 6** gives the conclusion of the thesis.



CHAPTER II

TEM and interpretation

2.1 TEM system

Optical microscope, which is a tool to magnify the scale of materials, has a resolution of about 250 nm, limited by wavelength of visible light. The light microscope is widely used because it is in the simplest form and easy to operate. Indeed, the restriction of instrument is a limitation of image resolution, which restricts observations of micro-structures of material. Thus, when the observations are in the atomic level, the light microscope is undesirable. However, micro-nanostructure of materials, which are an important issue to manipulate physical properties of materials, is still reaching to investigate. That is a major reason why transmission electron microscopy (TEM) is undertaken.

TEM is the premier tool for structural characterization of materials in nano-scale due to its high and ultra-high resolution, which is lower than 0.5 nm, and higher magnification of more than 100,000 times depending on an accelerating voltage. Also, the operating modes of TEM, such as electron diffraction (ED) pattern, diffraction contrast making images of defects, high resolution HR-TEM, are much useful. However, TEM system is much expensive and need the skills to prepare sample and interpret the results. In this chapter, the system and principle of TEM, operating mode, preparation of specimen, interpretation and other techniques are described.

To improve the image resolution and magnification, TEM uses electron instead of light because the wavelength of electron is lower than that of light. The lower wavelength of electron in TEM gives the image with higher resolution and higher magnification according to [26]

$$\delta = \frac{0.61 \lambda}{\mu \sin \beta}, \quad (2.1)$$

where δ is the resolution, μ is a refractive index of the medium (specimen), β is an angle of collection of the magnifying lens which is very small and λ is the wavelength of electron. All of these parameters are affected on the resolution of the microscope.

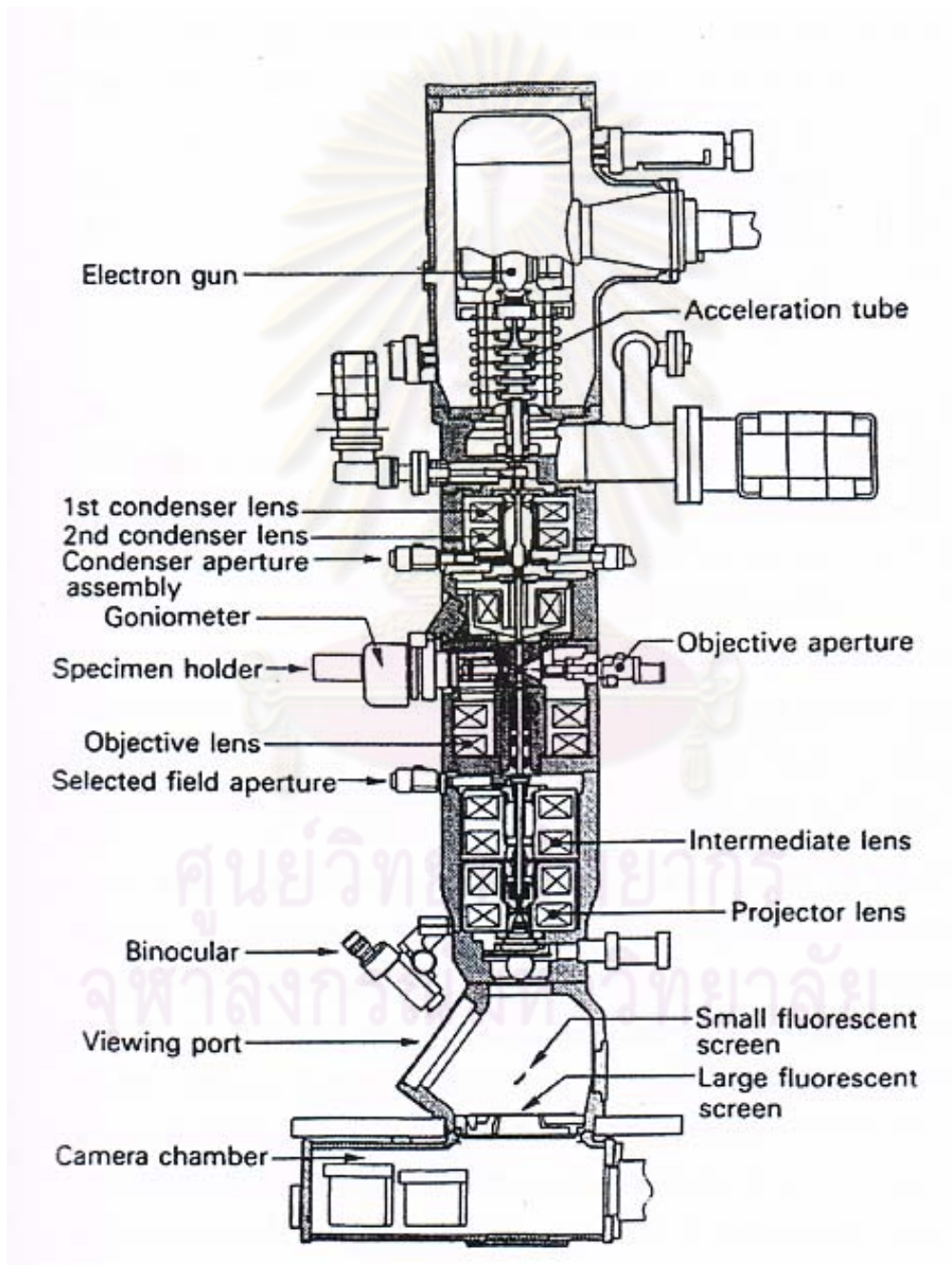


Figure 2.1: The main features of a conventional transmission electron microscope [25]

Figure 2.1 shows the main features of a conventional TEM system, which consists of three components. First component is the illumination system or the source of electrons. There are two types of electrons source in the TEM. The first type is thermionic source that produces electrons when heated. Another is a field-emission source that produces electrons when an intense electric field is applied. In Thailand, TEM uses only the thermionic source because even though the field-emission source could give increased efficiency but its operation cost is twice compared to a conventional TEM operating with the thermionic source. A comparison of the conventional electrons sources is shown in Table 2.1.

Table 2.1: The comparison of electron sources; thermionic tungsten filament, thermionic Lanthanum Hexaboride (LaB_6) and field emission [26]

Topic of the comparison	Electrons Sources		
	Thermionic:Tungsten Filament	Thermionic: LaB_6	Field Emission
Operating vacuum(mbar)	$10^{-4} - 10^{-5}$	$10^{-6} - 10^{-7}$	$10^{-9} - 10^{-10}$
Operating temperature (K)	2700	1700	300
Brightness ($\text{A}/\text{cm}^2 \cdot \text{ster}$)	$10^4 - 10^5$	$10^5 - 10^6$	$10^7 - 10^9$
Source Size (nm)	1×10^5	2×10^4	$< 1 \times 10^1$
Energy Spread (eV)	1-5	0.5-3	0.2-0.3
Probe Current Stability (% per minute)	0.1-1.0	0.2-2.0	2-10
Operating Life (hrs)	200	1000	3000
Cost (\$USD)	15	600	3000

Second component is an objective lens/stage, which is an important feature in TEM. The electrons moving from the source interact with specimen and get through the specimen showing the beam-specimen interaction on the back focal plane. This creates an electron diffraction (ED) pattern and selected-

area electron diffraction (SAD) pattern. The ED pattern consists of a bright central spot accumulating the direct electrons and a diffracted spot accumulating the diffracted electrons in each crystal plane.

Third component is the imaging system. When an aperture is inserted into the back focal plane of objective lens to choose bright central spot, then the aperture is blocking the diffracted beam and the direct beam go through to form image on the image plane. The image resulting from the direct beam is called “**a bright-field (BF) image**” whereas the diffracted spots were chosen the image resulting from their diffracted beams are called “**a dark-field (DF) image**”.

When the uniform electron beam transmits the specimen, its amplitude and phase can be changed. The uniform electron beam intensity will be transformed into a non uniform electrons beam intensity, which is observed on the viewing screen as a diffraction contrast. The diffraction contrast is usually consisted of *amplitude contrast* and *phase contrast*, which actually contribute to the image. Generally, the amplitude contrasts are attributed to a mass-thickness contrast and a diffraction contrast. The mass-thickness contrast is the most important in which of non crystalline materials such as polymers. On the other hand, the diffraction contrast is the most important in which of crystalline materials. So that the diffraction contrast is used as a tool to investigate, identify and distinguish structures of crystalline materials and extended defects in the crystal. Obviously, a *diffraction-contrast imaging* has been applied to complementary characterization in modes of BF and DF images.

ศูนย์วิทยทรัพยากร
จุฬาลงกรณ์มหาวิทยาลัย

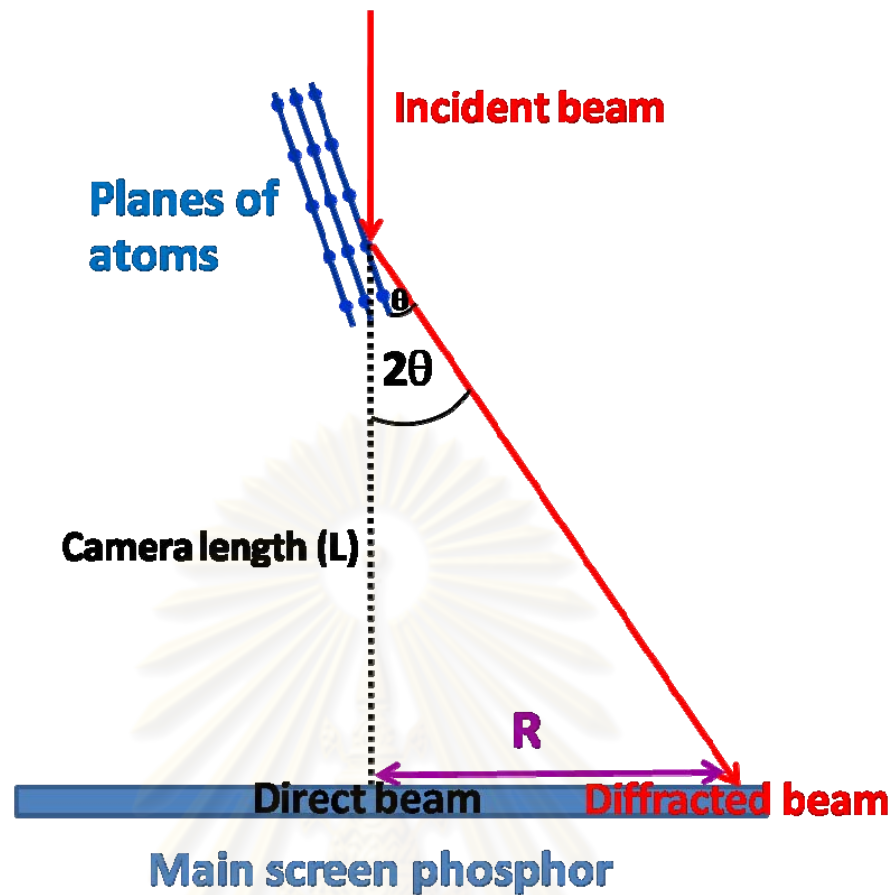


Figure 2.2: Schematic illustration of the incident electron beam and the diffracted electron beam in TEM [26]. R is a distance between the direct diffracted beams to the diffracted spots.

2.2 Interpretation of TEM results

2.2.1 Indexing of diffraction spots

After the incident electron beam was scattered from the planes of atoms, the electron beams diffracted from any (hkl) planes are represented as a pattern of bright spots on the viewing screen, as shown in Fig. 2.3. It is known that each diffraction spot gives information of the corresponding diffracted plane. Therefore, the indexing diffraction spots are needed.

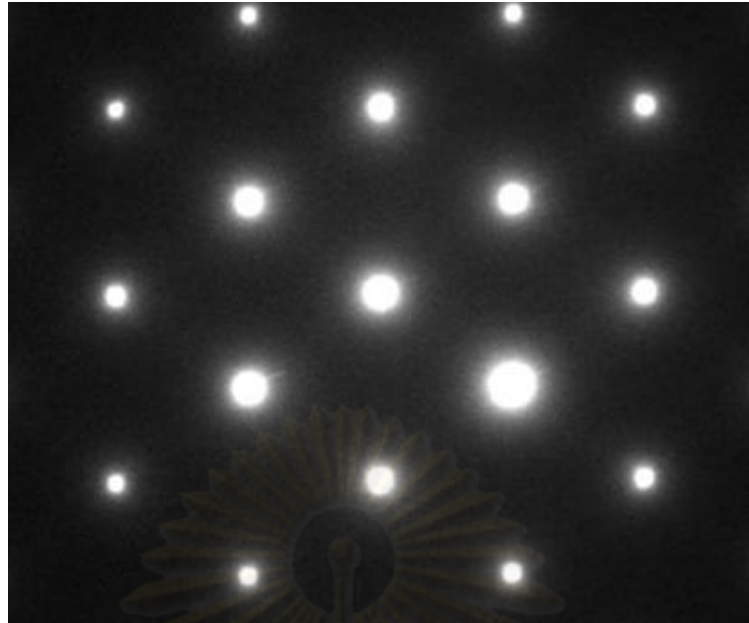


Figure 2.3: Electron diffraction pattern obtained from c-GaN crystal along the [110] zone axis

To index the diffracted spots, we start with the elastically scattered electrons which obey Bragg's condition.

$$2d_{hkl}\sin(\theta) = n\lambda, \quad (2.2)$$

which λ is wavelength of electrons, θ is Bragg's angle, n is an integer; when $n = 1$, d_{hkl} becomes an interplanar spacing of $(h \ k \ l)$ planes. In the case of cubic structure, the interplanar spacing of $(h \ k \ l)$ planes can be determined as follow

$$d = \frac{a}{\sqrt{h^2+k^2+l^2}}, \quad (2.3)$$

where a is a lattice constant of cubic lattice. When the Bragg angle θ is very small, $\sin(\theta)$ can be approximated to be θ . Then, Bragg's equation can be rewritten as

$$2d\theta = \lambda,$$

or

$$2\theta = \frac{\lambda}{d}. \quad (2.4)$$

As shown in Fig. 2.2, when the diffracted angle is very small or $R \ll L$, we get

$$2\theta = \frac{R}{L} \quad (2.5)$$

Then, equating the right hand side of Eq. (2.4) and Eq. (2.5) gives

$$\frac{R}{L} = \frac{\lambda}{d}, \quad (2.6)$$

$$Rd = L\lambda.$$

For the cubic structure

$$\frac{Ra}{\sqrt{h^2+k^2+l^2}} = L\lambda. \quad (2.7)$$

Finally, we obtain

$$R = \frac{L\lambda}{a} \sqrt{h^2+k^2+l^2}. \quad (2.8)$$

From Eq. (2.21), the distance R is directly depending on $\sqrt{h^2+k^2+l^2}$. To index the diffracted spots, for example, two of diffraction spots A and B are selected to measure the distance from the direct transmitted beam to the diffraction spots A (R_A) and B (R_B), as shown in Fig.2.4.

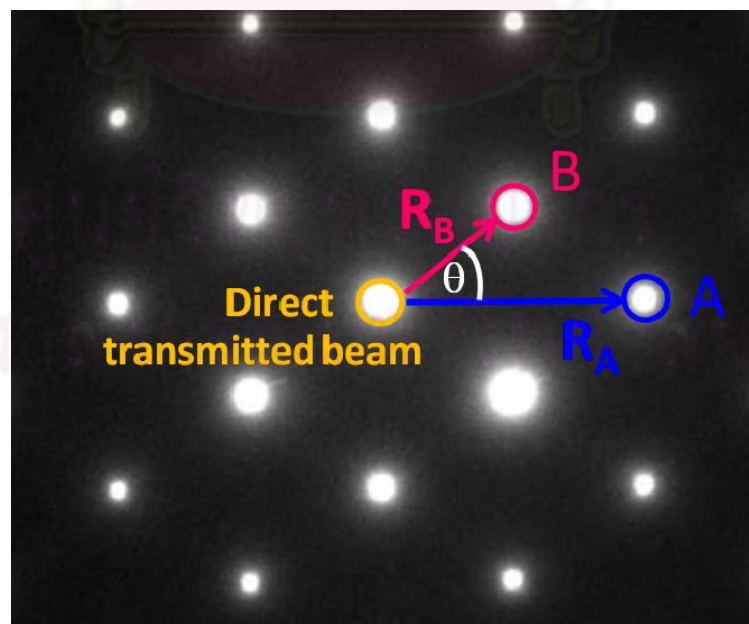


Figure 2.4: Distance between the direct transmitted beam and diffraction spot A and spot B indicating as R_A and R_B , respectively.

Table 2.2: The ratios of the reciprocal lattice spacing R_A/R_B

R	Spot A						
	{hkl}	{111}	{222}	{200}	{400}	{220}	{311}
Spot B	{111}	1	2	1.15	2.31	1.63	1.91
	{222}	0.50	1	0.58	1.15	0.82	0.96
	{200}	0.87	1.73	1	2	1.41	1.66
	{400}	0.43	0.87	0.50	1	0.71	0.83
	{220}	0.61	1.22	0.71	1.41	1	1.17
	{311}	0.52	1.04	0.60	1.21	0.85	1

In Fig. 2.4, distances from the central spot, which is represented the direct transmitted beam parallel to the [110] zone axis, to the diffraction spots A and B are R_A and R_B . The distances are known as the magnitude of reciprocal vectors R_A and R_B . From Eq. (2.21), the ratio of the reciprocal lattice spacing (R_A/R_B) as

$$\frac{R_A}{R_B} = \frac{\sqrt{h_A^2 + k_A^2 + l_A^2}}{\sqrt{h_B^2 + k_B^2 + l_B^2}} \quad (2.9)$$

Theoretical ratios of the reciprocal spacing of spots A and B diffracted from (hkl) planes in the cubic lattice are summarized in Table 2.2. After the measure of distances between the directed transmitted beam and the spot A spot B, the ratios of $\frac{R_A}{R_B}$, are taken to compare with the theoretical ratios in Table 2.2.

Finally, the indexing of spots A and B is confirmed by the scalar product to examine the angle θ between the reciprocal vectors R_A and R_B . The scalar product is

$$\mathbf{R}_A \cdot \mathbf{R}_B = |R_A| |R_B| \cos(\theta) \quad (2.10)$$

If the measured angle is corresponding to the calculated angle, the indexing will be accepted. Finally, the camera length, the electron wavelength and the measured spacing (R) are known then the lattice constant of the specimen can be determined by using the approximation of angle to calculating equation (2.8). Furthermore the diffraction spots shown on the diffraction pattern are indicated the quality of crystal plane. When the specimen is a high quality crystal plane which is perfectly parallel plane in real space, the diffraction spots diffracting from their planes are shown as a single sharply round spots whereas when the diffraction spots are shown with streak between any diffraction spots, there are represented that these spots are diffracted from the low quality crystal plane which is unparallel plane corresponding to the formation of some planar defects. The formation of streak is modification to the shape of reciprocal lattice points arising from the shape of crystal defects. The intensity distribution at a reciprocal lattice point is arising from the shape of stacking faults as shown in Fig.2.5.

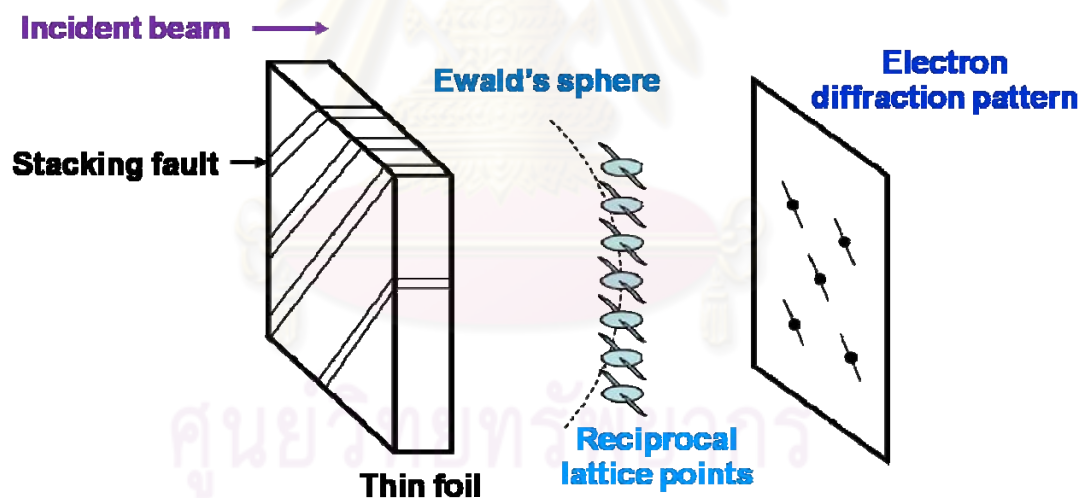


Figure 2.5: Streaking of reciprocal lattice points arising from precipitate plates lying parallel to the incident beam [27]

2.2.2 Diffraction-contrast imaging

Since in the operating mode of diffraction contrast; the electron diffraction pattern are shown in the back focal plane, the aperture is inserted to select the ED. If the bright central spot is selected, the image resulting from the direct beam will be demonstrated as BF-image on the main screen phosphor. BF

image contains planar defects information and the orientation information related to the selected area diffraction (SAD). In which resulting in a small part of the whole part of specimen and projecting 3-D specimen into 2-D image so the interpretation need to be careful. The imaging contrast represent in the strong or weak contrast refer to the density (number per unit area) of electrons hitting the detector not confusing with bright or dark.

If the diffracted spot is selected after the specimen, the image resulting from the selected spot will be demonstrated as DF-image on the main screen phosphor. DF image contains the specific orientation information resulting from the electrons in the strongly excited hkl beam was diffracted by a specific set of hkl planes and so the area that appears bright in the DF image is the area where hkl planes are at the Bragg's condition.



CHAPTER III

Experiments

In this chapter, the growth information and growth conditions of c-GaN on GaAs (001) and (311) substrates, the procedure of specimen preparation both plan-view and cross-section TEM specimen are described. The specimen preparation are optimized in each diamond grind sizes; 9, 6, 3, 1 and 0.5 μm . and controlled a speed of polishing; 60, 100 and 130 revolutions per minute (RPM) and observed by scanning electron microscopy (SEM). Subsequently, the macroscopic characterization of c-GaN on GaAs (001) and (311) is characterized by SEM and the microscopic characterization is characterized by plan-view TEM analysis.

3.1 MOVPE growth

In this work, all the c-GaN films were grown on GaAs (001) and (311) oriented substrates by metalorganic vapor phase epitaxy (MOVPE) at the laboratory of Prof. Dr.Kentaro Onabe, the University of Tokyo, Japan. The growth was performed with a low-pressure (160 Torr) MOVPE (an ULVAC system MPM-254). The MOVPE system consists of the horizontal growth reactor with a water-cooled cold wall. Radio frequency (RF) was used to heat the graphite subsector. There is no rotation of the substrate in this system. The reactor of MOVPE system used in this study is shown in Fig. 3.1.

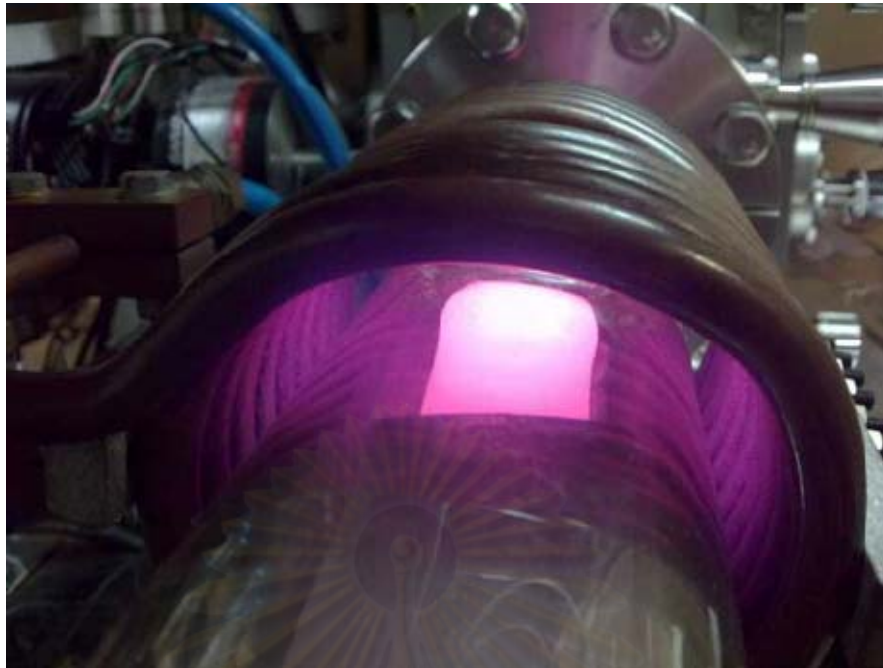


Figure 3.1: The horizontal reactor of MOVPE system at the University of Tokyo, Japan; 2010

A schematic diagram of growth system as shown in Fig. 3.2. High purity of Trimethylgallium (TMGa) was used as the precursor of Ga and Tertiarybutylamine (TBAs) and 1,1-dimethylhydrazine (DMHy) were used as the precursor of N. the temperature of bubbles of TMGa and DMHy were controlled at -10°C and 10°C , respectively. Pd-diffused H_2 as the carrier gas take the bubble of metalorganic liquids to the reactor and the precursors are decomposed above the substrate surface in the hot region.

After chemical cleaning of the GaAs substrate surface, a 100-nm-thick GaAs buffer layer was grown at 650°C to prepare the epitaxial surface, then an approximately 20-nm-thick low temperature GaN nucleation layer was grown at 575°C with concentration of group V/III ratio of 100. Finally, the c-GaN layer was deposited with different growth temperatures of 900 , 930 and 960°C . The other samples are the same procedure: a 100-nm-thick GaAs buffer layer was grown at 650°C to prepare the epitaxial surface then GaN nucleation layer was grown with different growth temperature of nucleation layer 550 , 575 and 600°C with V/III ratio of 100. And the c-GaN layer was deposited at 900°C as shown in Fig. 3.2. Typical growth rate was $6\ \mu\text{m}/\text{hour}$ examined by scanning electron microscopy (SEM) with V/III ratio was maintained at 25.

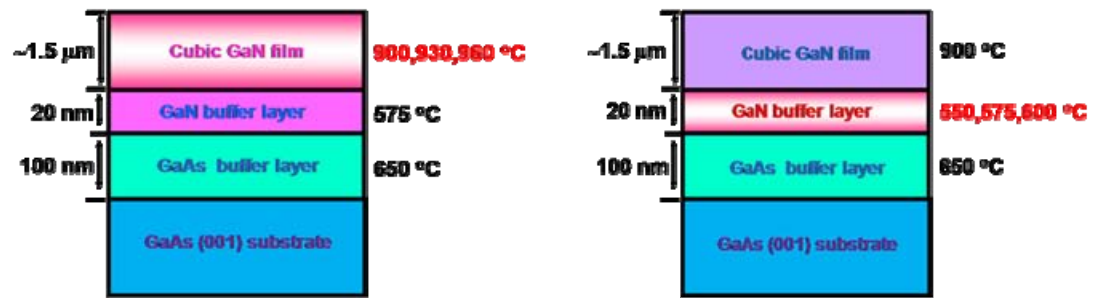


Figure 3.2: Sample model of c-GaN grown on GaAs (001) substrates with (left) different growth temperature 900, 930 and 960°C and (right) different growth temperature of nucleation layer 550, 575 and 600°C.

3.2 Preparation of TEM specimen

The specimen preparation for TEM depends on type of materials. In this research, the specimen is semiconducting materials which is hard and takes a long time to prepare. The semiconducting specimen must be thin relatively with electron transmit the specimen and the electron intensity falls on the screen enough to form the interpretable image. Generally, there is the axiom of TEM that “thinner is better”. The thickness of specimen should be < 100 nm which is possible to operate in TEM. In case of High Resolution TEM (HR-TEM) performed in atomic level which is showing on the lattice imaging need the specimen thickness < 50 nm. This thickness is not much important when the electron beam voltage increase but the specimen is risky damaged by electron beam. Otherwise, in the specimen preparation process there are essential conditions to beware of type of abrasive, grind size of diamond lapping film related to polishing speed, polishing force and polishing time and lubricant.

Ordinarily, there are two types of specimen preparation; plan-view preparation and cross-sectional preparation which are described as follows

3.2.1 Cross-sectional TEM specimen

The cross-sectional preparation of the semiconducting materials are prepared to study morphology of film epilayers including the interface through the surface, the formation of planar defects, dislocations and some defects may be embedded in film layer and the information of phase distribution and phase transition. Especially, the cross-sectional preparation process extremely depends on the properties of film and substrate materials. In this research, the film and substrate materials are GaN and GaAs, respectively. The hardness of single-crystal at room temperature GaN shows higher hardness than GaAs so the preparation process must be carefully and need the great skills to get the thickness in nano-scale with the smooth surface and completely whole layers. The preparation process involves cutting, clamping, polishing and precision ion polishing process.

Cutting process

First of all, the specimen surface is cleaned by acetone. Then the specimen is cut by a diamond pen to the width of specimen below 1 mm. or the specimen is cut by a diamond-wheel saw and stuck on a microscope slide by Kenji glue and heated in a hot oven at 80°C for 30 minutes. Then the specimen is cut by the diamond-wheel saw as shown in Fig. 3.3 to the width of specimen is below 1 mm

Clamping process

After the specimen was cut, the two pieces of cut specimen which was wiped the specimen surface by acetone are stuck film's side together by high performance epoxy resin: M-BOND 610 glue. The stuck specimen as shown in Fig. 3.4 is clamped by a clamping holder and heated by a hot oven at 170°C for 24 hours.



Figure 3.3: The model 650 low speed diamond wheel saw.



Figure 3.4: Sample model of the two pieces of specimen are stuck by M-BOND glue



Figure 3.5: (left) The specimen is polished by the 9 μm diamond lapping film on the polisher, (right-top) Sample model of the clamped specimen is stuck on a triangular shaped glass and (right-below) showing the diamond grind size of diamond lapping films.



Figure 3.6: Precision Ion Polishing system (PIPs)

Polishing process

After 24 hours of heating the clamped specimen, waiting for its cooled down then the clamped specimen is stuck by Kenji glue on a triangular shaped glass (as shown in Fig. 3.5 (right-top)), polished by abrasive sand paper disc to get rid of the sharpness of glass which is risky damaging the specimen, and heating at 80°C for 30 minutes again. Then the specimen is polished by the diamond lapping film (as shown in Fig. 3.5 (right-below)) with 9 µm diamond grind size to decrease the specimen thickness. Next the specimen is polished by 6 µm diamond grind size that we are polishing until the scratch of the previous diamond grind size is disappear and then changing to the smaller diamond grind size until 0.5 µm. While we are polishing with 0.5 µm diamond grind size, the specimen should be approximately a half of its original thickness. After that turn the specimen over and the polishing process is running again and starting 9 to 0.5 µm diamond grind size which the other surface is extremely thin making the polishing with difficulty and carefulness. The specimen is polished until the specimen thickness is approximately 50 µm.

Precision ion polishing process

When the thinnest specimen could be tried to polish, a suitable copper grid is stuck on the polished specimen with M-BOND glue and heating the polished specimen with copper grid at 170°C for 2 hours. Then taking a while to cool down and using acetone to take apart the specimen on copper grid from the triangular shaped glass. Finally, the specimen on copper grid is milled by Precision Ion Polishing system (PIPs) as shown in Fig. 3.6 which can control ion beam angle, time and voltage depending on the specimen thickness. The milled specimen on copper grid is readily to TEM operation.

3.2.2 Plan view TEM specimen

The plan-view preparation of semiconducting materials is prepared to study surface morphology, dislocations planar defects and microstructural defects in the direction normal to the layer surface. The plan-view preparation process is the same as the cross-sectional preparation in the process of cutting and PIPs. However, the clamping is not necessary whereas the polishing process is still running which the film's side of specimen is stuck on the triangular shape glass by Kenji glue, heated at 80°C for 30 minutes and polished until the specimen thickness is approximately 50 μm without turn over the other side. In the case of plan-view preparation we try to polish the substrate from the film and finally, we keep only the film layer stuck on the triangular shape glass.

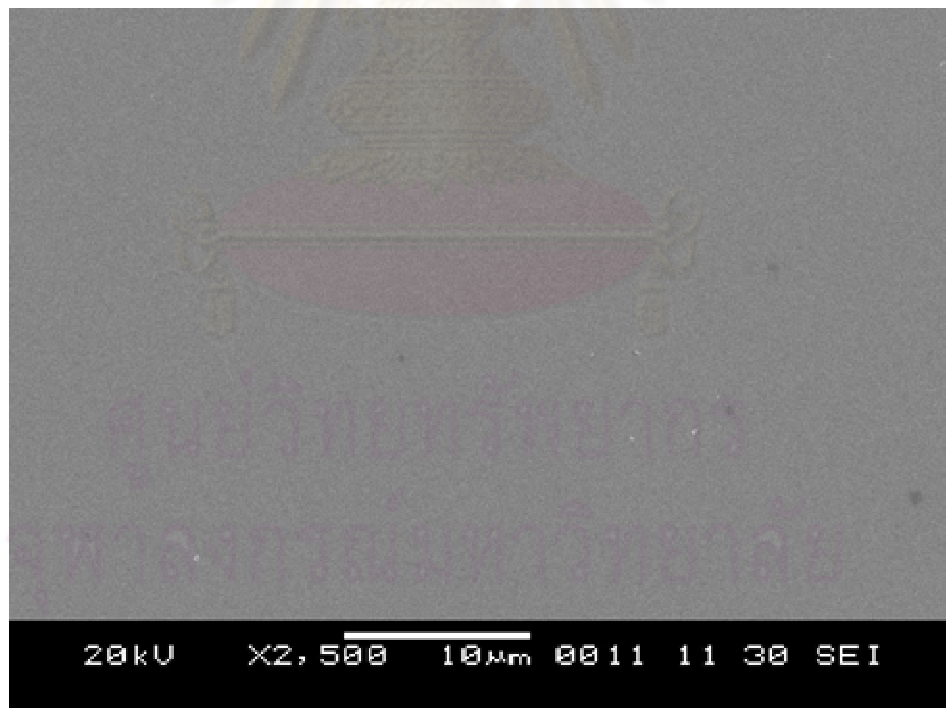


Figure 3.7: The surface of GaAs substrate surface, using as the specimen to optimize polishing process, without any polishing.

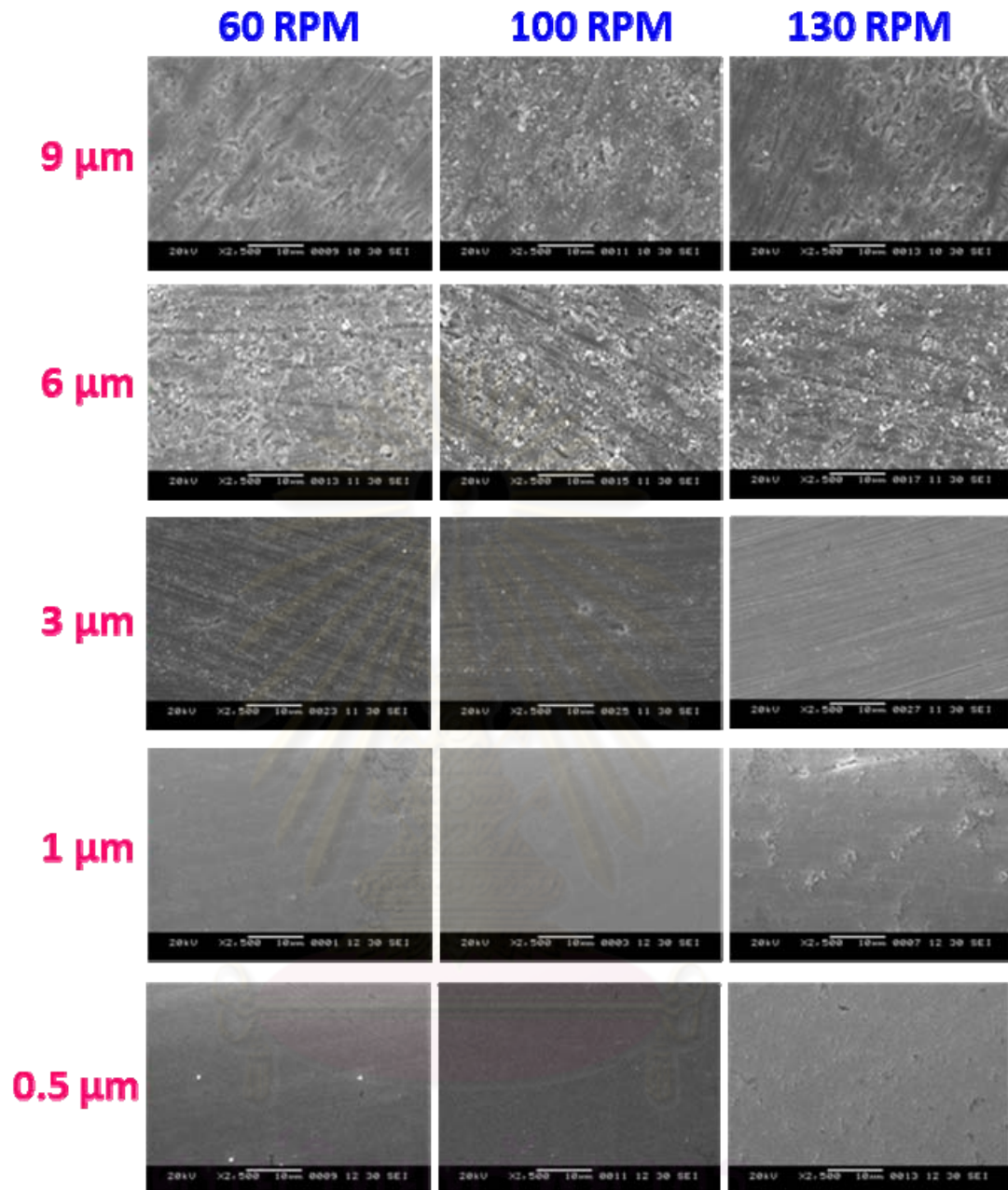


Figure 3.8: Plan view SEM images showing the surfaces of specimens, which were polished by diamond-lapping films with different diamond grind sizes (0.5, 1, 3, 6 and 9 μm) and various speeds of the polisher (60, 100 and 130 rpm).

3.3 Optimization of polishing process

Before the c-GaN preparation process will be really started, the optimize polishing which is relatively observed with different diamond grid size of

diamond lapping film and speed of polisher is needed to learn skills and determine suitable speed of polisher. In details, GaAs substrates are stuck on the triangular shape glass, prepared as the plan-view TEM specimen preparation and polished by the diamond films with 9, 6, 3, 1 and 0.5 μm of diamond grind size and the speed of polisher; 60, 100 and 130 RPM, then the surface of specimen is observed by scanning electron microscopy (SEM). First of all, Fig. 3.7 showing the surface of GaAs substrate, without any polishing, is perfectly smooth as shown in SEM image then Fig. 3.8 as shown in series of SEM images demonstrating the surfaces of specimen which are polished. It can be observed that the specimen is rough with facets resulting from the scratches of diamond grid size. For the specimen is polished by 9 and 6 μm diamond films, the roughness of surface is decreased with increasing the speed of polisher. This may result from the scratches which are clearly seen in the factors of size and direction. The slow speed of polisher has an influence to control the specimen which is directly affected on the surface and the GaAs perfect smooth surface is still affected. For the middle size of diamond grind, the highest speed is resulting in the smoothest surface which is obviously seen. Finally, the fine diamond grind size is compatible with 100 RPM of speed polisher which the surface of specimen has less the scratch and less any roughness. The results are reasonable in each conditions of polishing both the effect of previous surface and the effect of the friction happening between the fine diamond grind size and the surface are shown on the SEM imaging in each process.

CHAPTER IV

Microstructural Characterization of c-GaN on GaAs (001)

4.1 Sample Structure and Growth Conditions

According to roles of the low temperature buffer layer, which is used as the the protection layer of substrate surface and the nucleation layer, the optimum growth conditions of the low-temperature grown GaN buffer layer (LT-GaN buffer) is required for the growth of c-GaN films with higher cubic phase purity. In Chapter IV, we selected the cubic GaN (c-GaN) films grown with different growth temperatures (550, 575 and 600°C) of LT-GaN buffer. Figure 4.1 shows schematic drawing of sample structure. As seen in the Fig. 4.1, firstly, a 100-nm-thick GaAs buffer layer was grown on GaAs (001) substrate at 650°C. Secondly, a 20-nm-thick of LT-GaN buffer was grown at temperature in the range of 550-600°C. Finally, a 1.5- μm -thick c-GaN film was grown on top at 900°C [29, 30, 31, 32].

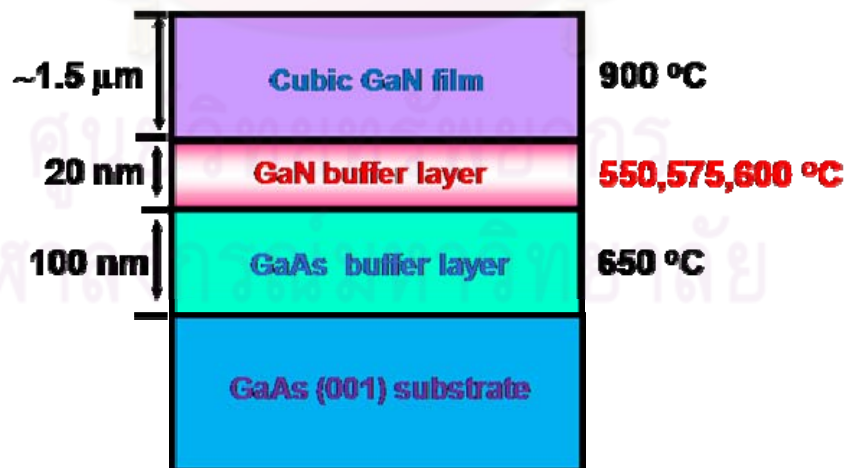
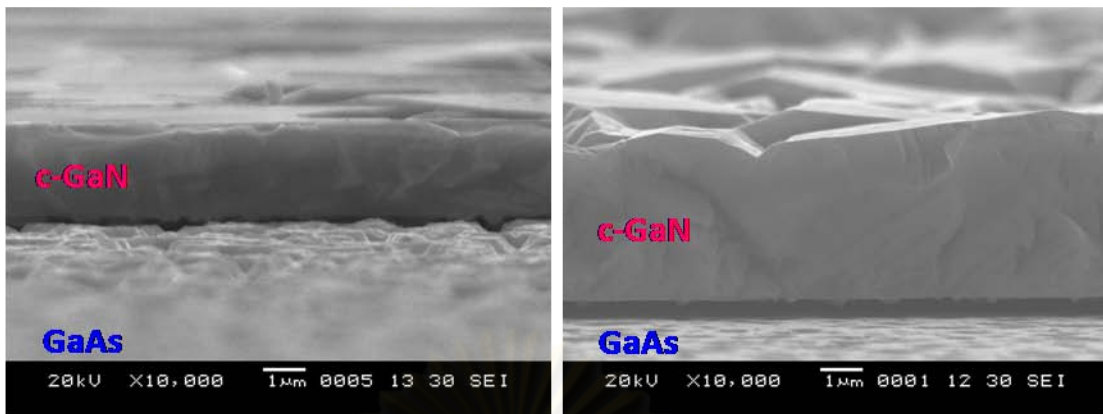
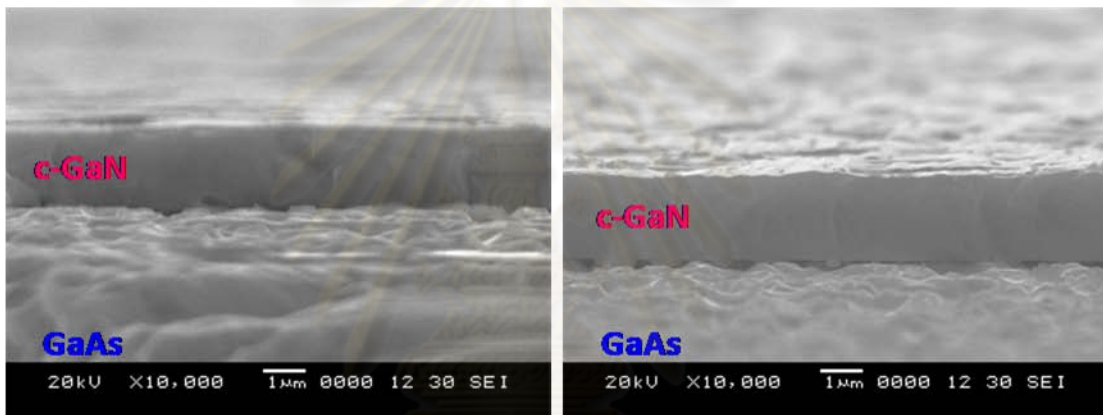


Figure 4.1: Schematic drawing of c-GaN sample grown on GaAs (001) substrate with different growth temperatures of LT-GaN buffer; 550, 575 and 600°C.

$T_s(\text{buff.}) = 550^\circ\text{C}$



$T_s(\text{buff.}) = 575^\circ\text{C}$



$T_s(\text{buff.}) = 600^\circ\text{C}$

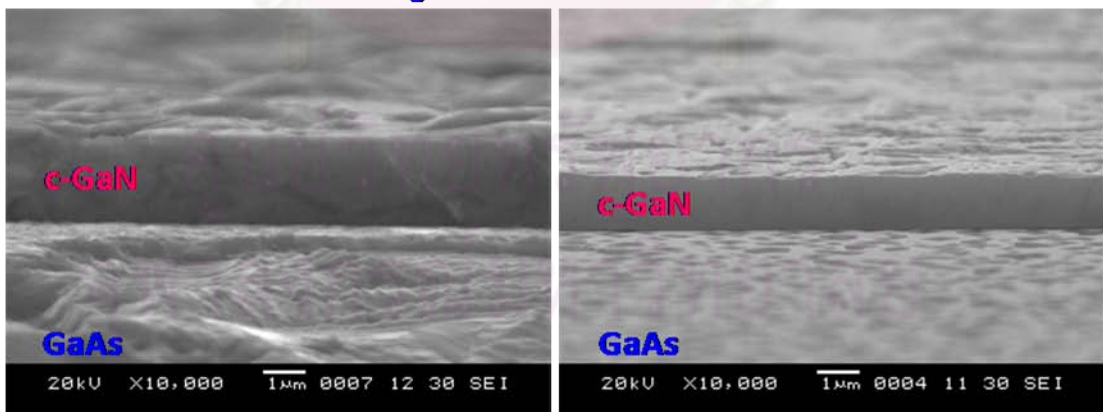


Figure 4.2: SEM images showing a cross-section of the c-GaN films grown on GaAs (001) substrates with different growth temperatures of LT-GaN buffer; 550, 575 and 600°C.

4.2 Morphologies of Surface and Interface

The GaAs substrate surface is still smooth (as shown in Fig. 3.7) until deposition of high-temperature of c-GaN films layer. A low sublimation point of As is causing the GaAs substrate surface degradation at high substrate temperature affecting on the GaN main layer. The GaAs pre-layer is needed as a protection layer to protect As thermal decomposition and expand to improve the GaN main layer and to reduce the effects of residual oxygen on the GaAs surface affecting on the nitride layer [29]. The GaAs buffer layer is usually grown at 600-700°C and 200 nm thick [30]. After the GaAs pre-layer is deposited, the LT-GaN buffer layer is depositing to maintain an automatically GaAs smooth surface and Trampert *et al.* [31] and Brandt *et al.* [32] found that GaN nucleates in the cubic phase on automatically smooth 100 nm-thick GaAs (001) pre-layer. The degradation of GaAs surface at the GaN/GaAs interface has taken to seeds of formation of structural defects; stacking faults (SFs), twins, hexagonal inclusions, dislocations (DTs) etc. The GaN buffer layer working as the nucleation layer grown at low-temperature; 550, 575 and 600°C are characterized and compared which one can improve the GaN main layer grown at high temperature (~900°C) and relatively can protect the GaAs surface from the thermal decomposition. Figure 4.1 demonstrates the SEM images of cross-section of the c-GaN films grown on GaAs (001) substrates with different growth temperatures of LT- GaN buffer; 550, 575 and 600°C. For the T_g (buff.) = 550°C voids can be observed at the GaN/GaAs interface. The occurrence of such voids is considered to relate the deposition of GaN buffer layer with low temperature and high growth rate. The formation of GaN buffer layer is non-uniformity like a mountain while the GaN main layer is growing, there is an influence of thermal energy to recognize the GaN buffer layer. The remains which were not rearranged are resulting in these voids. For the T_g (buff.) = 600°C correlation between the deposition of GaN buffer layer with high temperature and the uniformity of these layers evidence there are voids not like a mountain shape can be observed at the GaN/GaAs interface. The rearrangement of GaN buffer layer with low growth rate has migrated to be single crystal and have the uniformity although the GaN buffer layer maybe not covered the GaAs surface which is

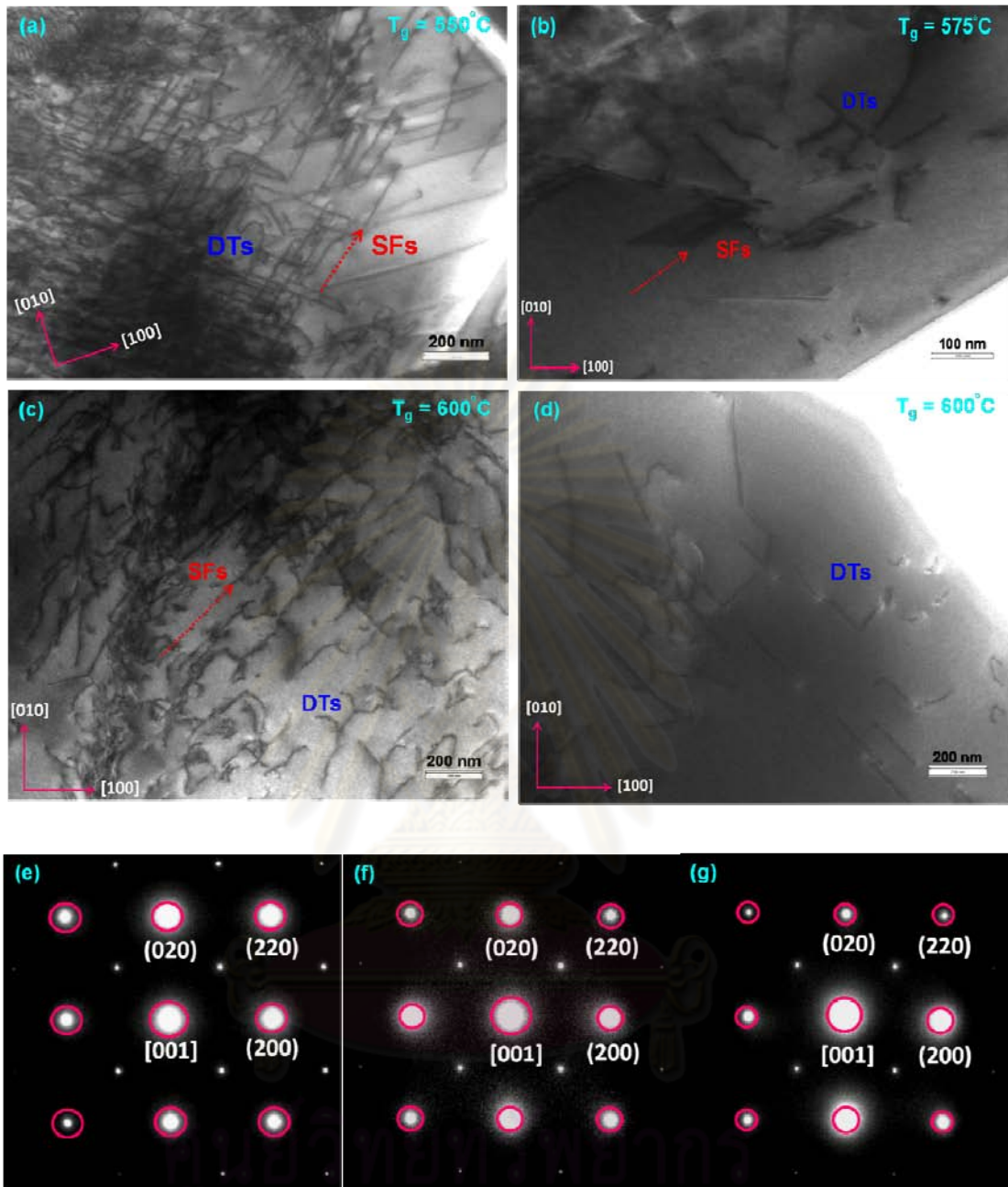


Figure 4.3: TEM images showing plan-view micrographs and ED patterns of the c-GaN films grown with different growth temperature of GaN buffer layer; (a), (e) 550°C, (b), (f) 575°C and (c), (d), (g) 600°C.

imperfection of the protection layer. When its imperfection occurs, the V-shape voids causing from thermal decomposition of As can be observed. As the results c-GaN with the T_g (buff.) = 575°C is predicted to be a candidate growth

temperature of GaN buffer layer affecting on the quality of cubic phase GaN main layer and is supported by the plan-view TEM images as shown in Fig. 4.3 and the cross-sectional TEM analysis will be describing in topic 4.3

Figure 4.3 shows the plan-view TEM micrographs and electron diffraction (ED) patterns of c-GaN grown on GaAs (001) substrates with different growth temperature of GaN buffer layer. For the $T_g(\text{buff.}) = 550^\circ\text{C}$ shown in Figs. 4.3 (a) and (e) high density of stacking faults (SFs) and dislocations (DTs) are observed. The SFs are clearly seen and elongated along the [111] direction. The existence of SFs and DTs are consistent with the voids which were found in cross-section SEM images. For the $T_g(\text{buff.}) = 600^\circ\text{C}$ shown in Figs. 4.3 (c), (d) and (g) the mixing zone are observed such as there are a high density of SFs and DTs as shown in Fig. 4.3 (c) which is probably found hexagonal inclusions and the another zone contains only the DTs as shown in Fig. 4.3 (d) where the SFs are invisible. For the $T_g(\text{buff.}) = 575^\circ\text{C}$ as shown in Figs. 4.3 (b) and (f) is showing the wide SFs which are observed that these broad lines are not expanding to the GaN surface. The DTs are less found than the others temperature.

4.3 Generation of defects in c-GaN with different growth temperature of GaN buffer layer

The specimen; c-GaN grown on GaAs (001) substrates with different growth temperature of GaN buffer layer; 550, 575 and 600°C were prepared by the cross-sectional TEM preparation process and characterized by TEM analysis as follows:

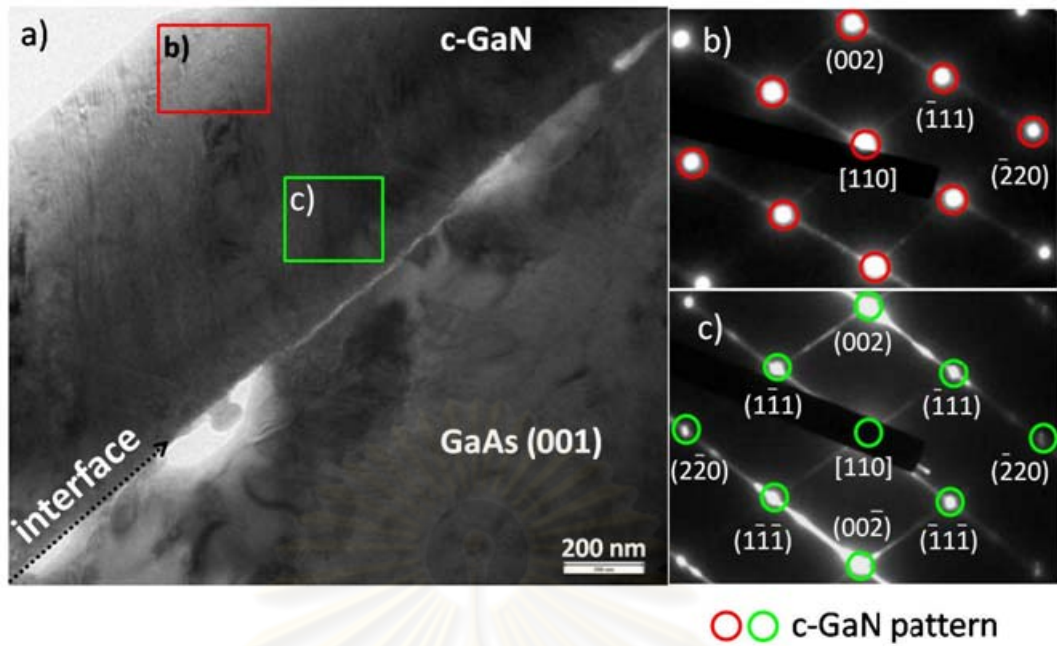


Figure 4.4: Cross-sectional TEM micrographs and ED patterns of c-GaN layers grown on GaAs (001) substrates with growth temperature of GaN buffer layer at 550°C.

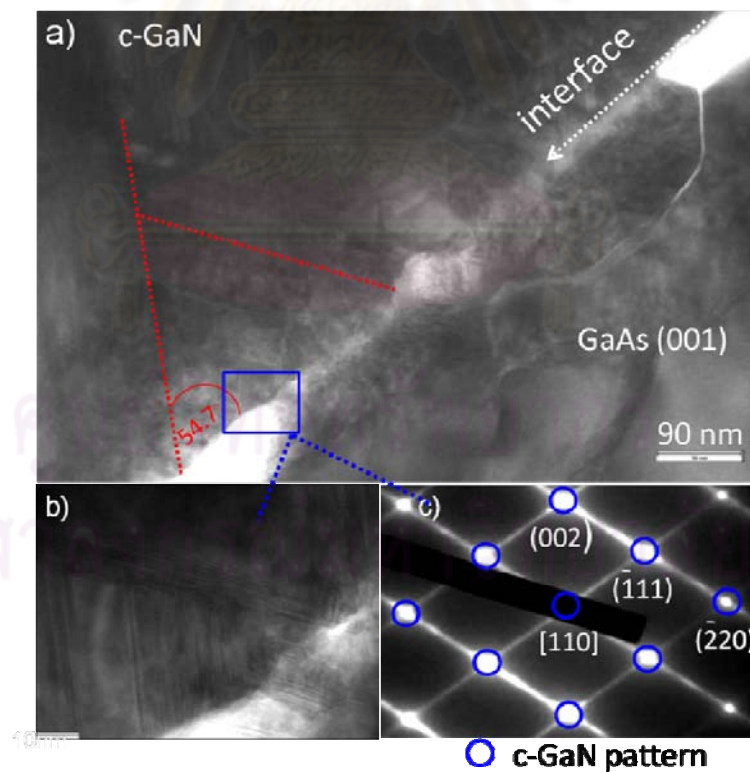


Figure 4.5: Cross-sectional TEM micrographs and ED patterns of c-GaN layers grown on GaAs (001) substrates with growth temperature of GaN buffer layer at 550°C have taken at the GaN/ GaAs interface.

The ED pattern shown in Fig. 4.5 (c) demonstrated different type of single diffraction spots which include the high intensity of streaking. These intensity are indicated that the high density of SFs become dense into the hexagonal phase single crystal. As showing on the micrographs (in Figs. 4.5 (a) and (b)) the SFs which are generated from the GaN/GaAs interface and the generation of SFs refer to the direction of hexagonal inclusions increasing with the thickness of films layer. The formation of these defects is caused by the imperfection of surface in the GaN buffer layer.

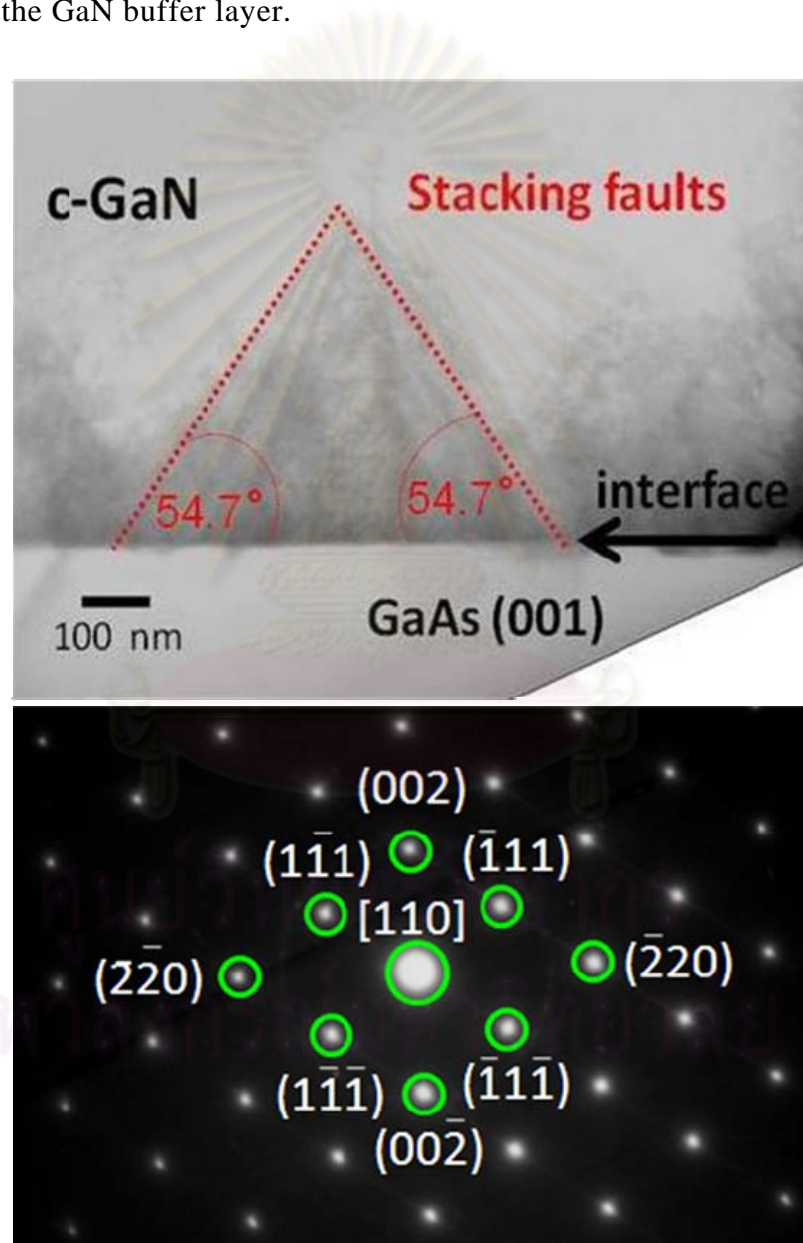


Figure 4.6: Cross-sectional TEM micrographs and ED patterns of c-GaN layers grown on GaAs (001) substrates with growth temperature of GaN buffer layer at 575°C

For the growth temperature of GaN buffer layer grown at 575°C, the selected-area diffraction (SAD) pattern at the GaN/GaAs interface as shown in Fig. 4.6 (b) showed no diffraction types of single diffraction spots so the GaN close to the GaN/GaAs interface has the cubic structure. The micrograph (in Fig. 4.6 (a)) is characterized by a pyramid like structure showing (1-11) and (-111) facets which represent the SFs close to the GaN/GaAs interface.

For the highest growth temperature of GaN buffer layer, obviously the planar defects have a highest density than the growth temperature of GaN buffer layer grown at 550°C and 575°C. These defects looking like penetrating into the GaN surface and voids have V-shape (in Fig. 4.8) which were caused by the thermal decomposition of As. The TEM micrograph (in Fig. 4.7 (a)) is clearly seen separating zones as in Figs. 4.7 (b), (c), (d) and (e) which are characterized by the horizontal stripes and the stripes of planar defects. Corresponding to the ED pattern in each zone, Fig. 4.7 (b) SAD near the GaN surface there is no the streaking of diffraction spots so GaN has the pure cubic structure, Fig. 4.7 (c) SAD in the middle of GaN main layer near the stripes of planar defects there is the streaking of diffraction spots dense into the diffraction spots of hexagonal phase single crystal indicating GaN has the cubic structure and the hexagonal phase inclusions, Fig. 4.7 (d) SAD in the stripes of planar defects is showing the streaking of diffraction spots and the diffraction pattern of hexagonal phase single crystal, then the crystal orientation of h-GaN is growing up along the [1-11] direction so the Fig. 4.7 (d) zone is the mixing region of c-GaN/h-GaN, and Fig. 4.7 (e) SAD near the GaN/GaAs interface there are the streaking of diffraction spots and hexagonal phase inclusions.

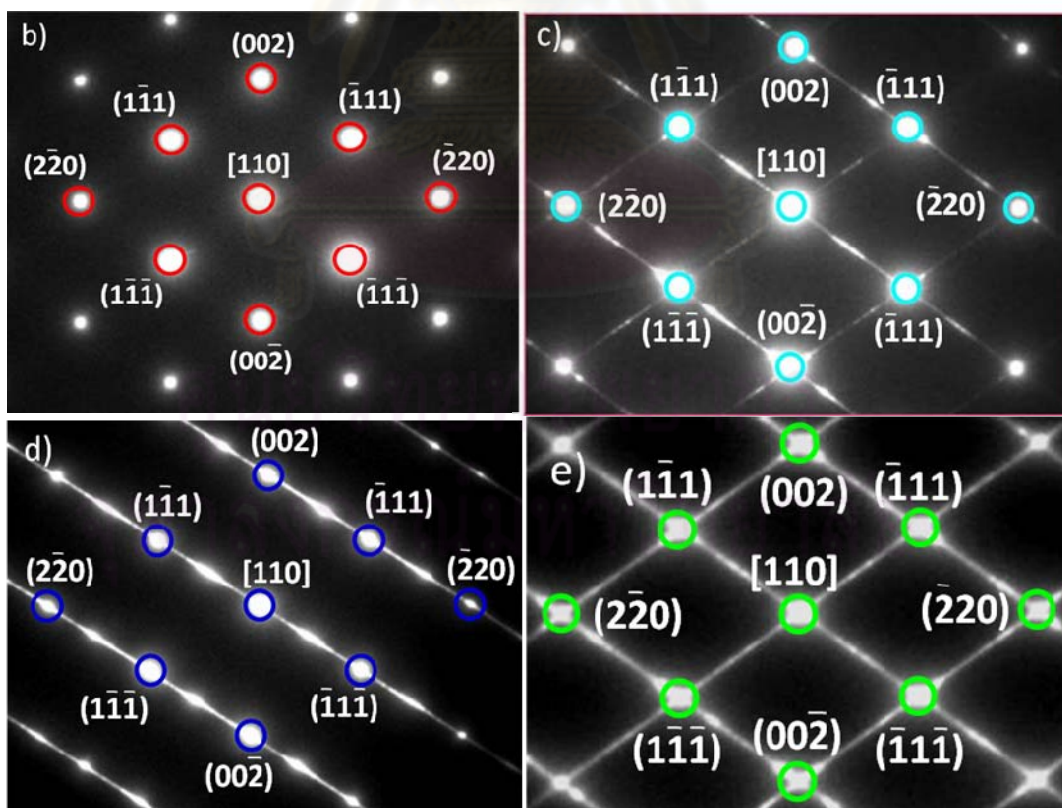
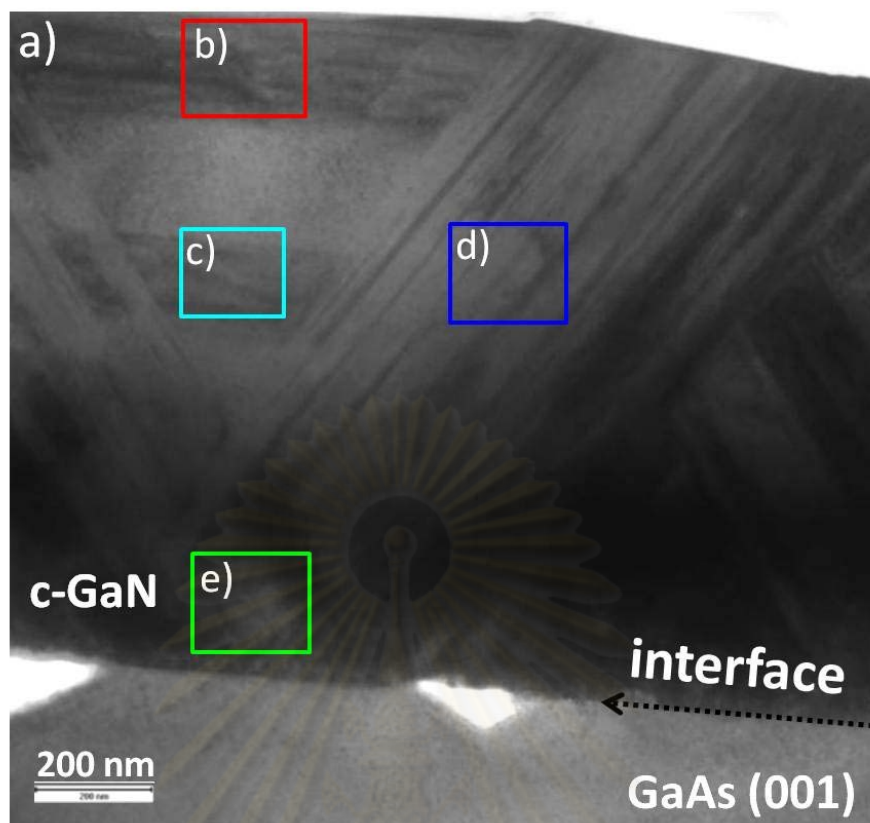


Figure 4.7: Cross-sectional TEM (a) micrograph and (b), (c), (d) and (e) ED patterns of c-GaN layers grown on GaAs (001) substrates with growth temperature of GaN buffer layer at 600°C.

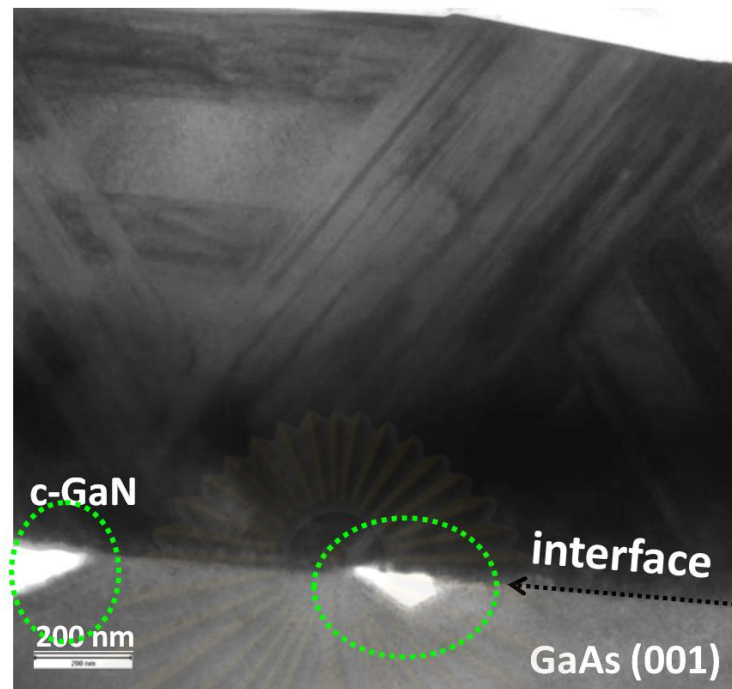


Figure 4.8: Cross-sectional TEM micrograph of c-GaN layers with growth temperature of GaN buffer layer at 600°C is highlighting at the V-shape voids which were caused by the As thermal decomposition.

In order to verify the existence of the planar defects, the dark-field (DF) cross-sectional TEM images of c-GaN grown on GaAs (001) substrates with different growth temperature of GaN buffer layer at 550°C (in Fig. 4.9 (a)), 575°C (in Fig. 4.9 (b)), 600°C (in Fig. 4.9 (c)) which have taken from the diffracted spot (in Fig. 4.10 (a)) in the diffraction pattern of hexagonal phase single crystals shown in Fig. 4.10 (b) have been used to analysis. In bright-field (BF) TEM image, the dark-constrast region related to the specimen and the bright-constrast region related to the direct electron beam is falling on the main screen phorphos or meaningless. On the otherhand in the DF-TEM image, the bright-constrast region related to c-GaN films which is diffracted from the selected diffraction plane so the DF-TEM image is advantage to investigate and characterize the existence of the hkl planes of c-GaN such as {111} facets are identified the existence of SFs.

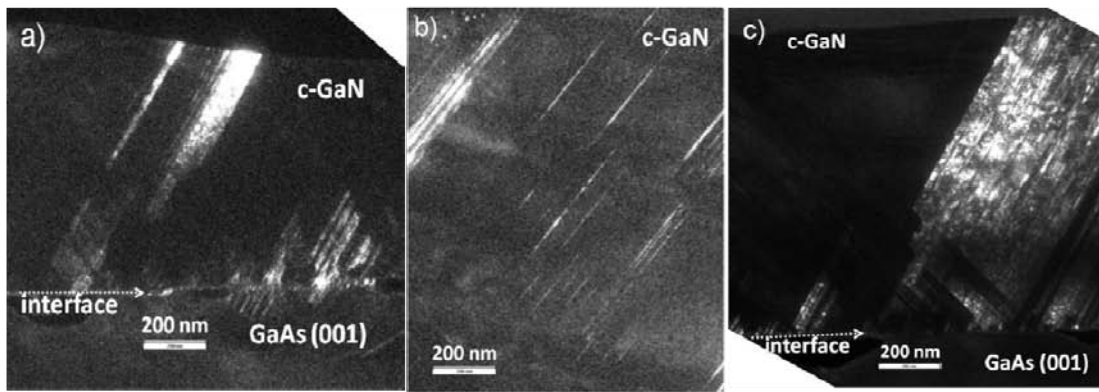


Figure 4.9: Dark-field (DF) images of c-GaN on GaAs substrates with different growth temperature of GaN buffer layer at (a) 550°C, (b) 575°C and (c) 600°C taken from the (1-100) of hexagonal diffraction spots near the (1-1-1) of cubic diffraction spots

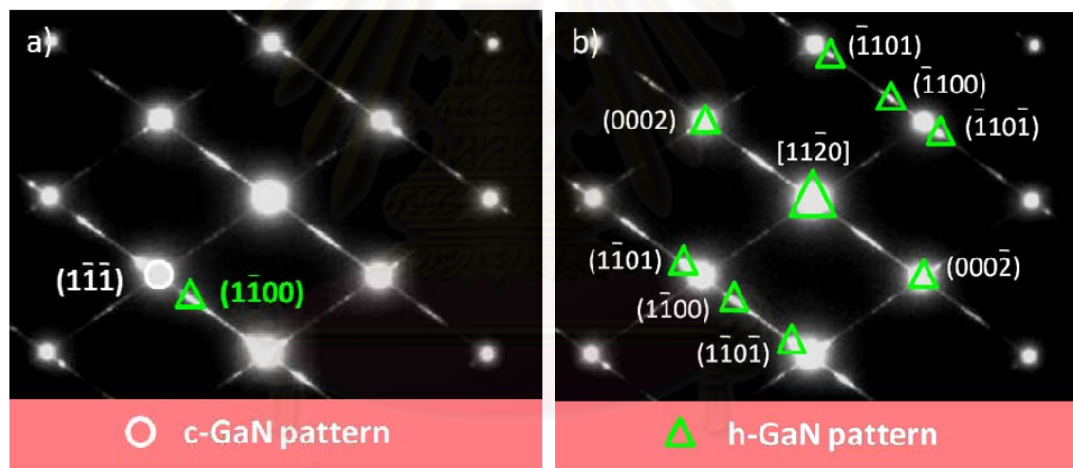


Figure 4.10: ED pattern of (b) cubic single crystal and hexagonal single crystal showing (a) the (1-100) of hexagonal diffraction spots near the (1-1-1) of cubic diffraction spots taken to form DF images in Fig. 4.9

Figure 4.9 represent the existence of SFs. Obviously in the Figs. 4.9 (a) and (c) a high density of SFs is observed and the formation of SFs is generated from the GaN/GaAs interface and penetrating into the GaN surface. For the growth temperature of GaN buffer layer at 575°C there is a density of SFs less than another. So the amount and the distribution of such extended defects

seriously affects on the crystalline quality resulting from the DF-TEM images are confirmed that the optimum temperature of the growth temperature of GaN buffer layer is 575°C to obtain the higher quality of the c-GaN layers.

4.4 Growth conditions of c-GaN on GaAs with different growth temperature of film epilayer

According to the As thermal decomposition occurs at high growth temperature, the growth temperature of GaN films layer is the important parameter that we are seeking for the optimum temperature to grow cubic GaN films phase purity. The sample conditions of c-GaN firstly, a 100 nm of GaAs buffer layer grows on GaAs (001) substrate at 650°C, next a 20 nm thick of GaN buffer layer grows at 575°C and finally, the 1.5 μm of cubic GaN films grow at 900, 930 and 960°C as shown in Fig. 4.11.

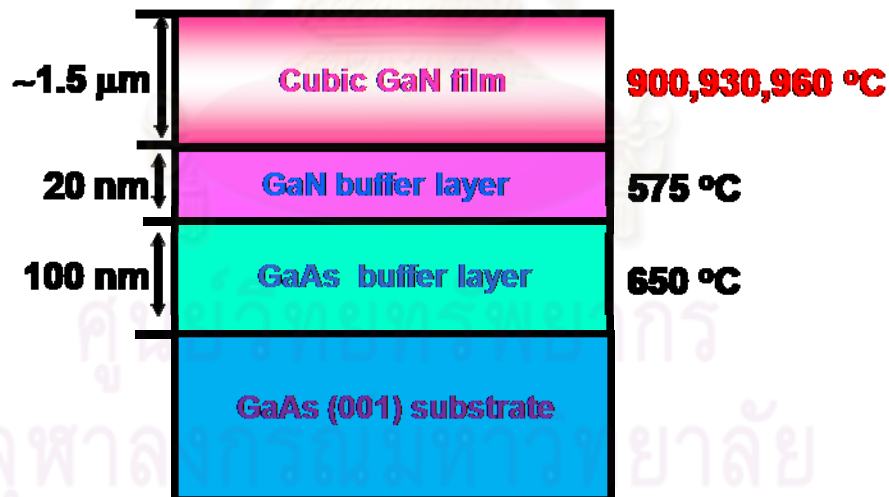


Figure 4.11: Sample model of c-GaN grown on GaAs (001) substrates with different growth temperature of films layer 900, 930 and 960°C.

4.5 Microstructural investigation of c-GaN on GaAs (001) substrate with different growth temperature of film epilayer

The specimen; c-GaN grown on GaAs (001) substrates with different growth temperature of film epilayer 900, 930 and 960°C were prepared by the cross-sectional TEM preparation process and characterized by TEM analysis as follows:

Figures 4.12 (a) and (d) present a cross-sectional TEM micrograph and an ED pattern of c-GaN layer grown at 900°C. We found that stacking faults are characterized by a high density of pyramid like structure showing the (1-11) and (-111) facets (Fig. 4.12 (a)) with an angle of 54.7° inclined from the (001) substrate surface. It is seen in the ED pattern in Fig. 4.12 (d) that there is a weak streak connecting the (111) reciprocal lattice points to the (002) and (220) points. Noted that no single diffraction spots related to hexagonal phase, which are expected to appear near the (111) spots, was observed.

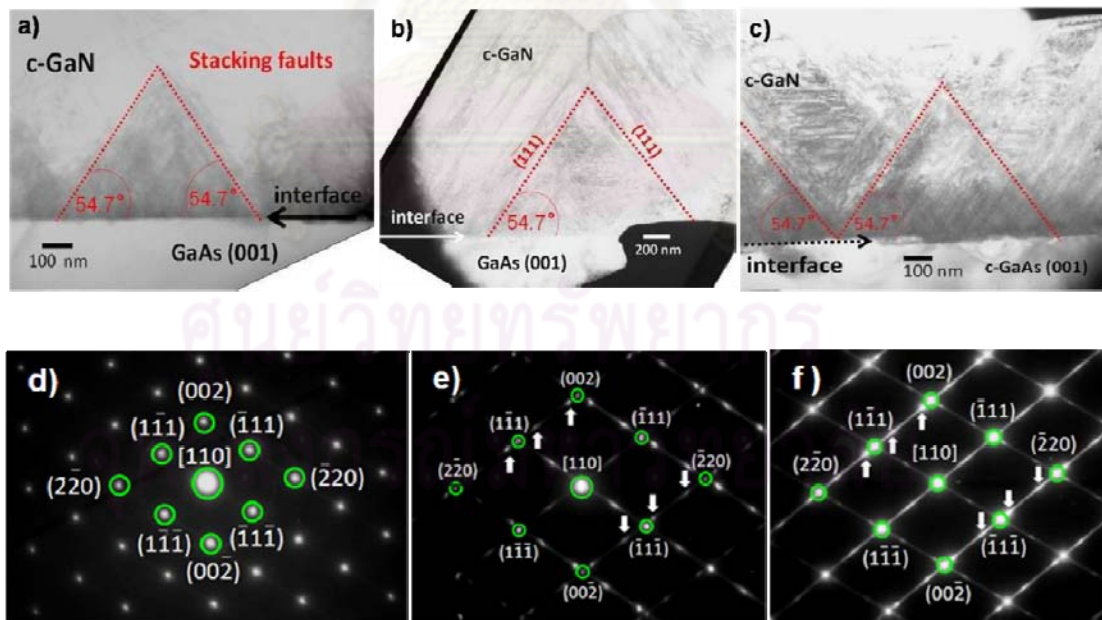


Figure 4.12: Cross-sectional TEM micrographs and ED patterns of c-GaN layers grown on GaAs (001) substrates with growth temperature of films epilayer; (a), (d) 900°C, (b), (e) 930°C and (c), (f) 960°C with key-diagrams. The arrows indicate the positions of diffraction spots for the hexagonal phase single crystal.

These demonstrated an incorporation of only SFs with extinction of hexagonal phase single crystal in the c-GaN layer grown at 900°C.

For higher growth temperature of 930°C, the ED pattern shown in Fig. 4.12 (e) exhibited a different type of diffraction spots as indicated by arrows. These extra spots are connected with the streak lines through the cubic (111) spots. Such different ED pattern represents a mixed cubic/hexagonal phase in the grown layer. It is also clearly seen in TEM micrograph shown in Fig. 4.12 (b) that microstructures, which are consisted of the (1-11) and (-111) faceted pyramid like features as the same in the layer grown at 900°C. This demonstrates an existence of hexagonal phase single crystal regions associated with a generation of SFs along the $\langle 111 \rangle$ directions.

For the highest growth temperature; 960°C the obvious streak lines connected between the diffraction spots becomes more intense compared to the layers grown at lower growth temperatures. Intensity of the extra diffraction spots is significantly increased as shown in Fig. 4.12 (f), indicating the present of single crystal h-GaN in the c-GaN matrix. TEM micrograph shown in Fig. 4.12 (c) illustrates higher density of SFs, which is indicated by an increase in a density of line contrasts parallel to $\{111\}$ planes. Looking like these lines are started from the (111)-steps on the GaN/GaAs interface and penetrating into the layer.

Since, the GaAs substrate surface is very unstable at such high growth temperatures, it is evidenced that the hexagonal inclusion is initiated from the formation of SFs, which is related to the formation of (111)-steps on the substrate surface during the growth at relatively high temperatures ($>900^\circ\text{C}$). Even though, to prevent from thermal decomposition, a two step growth process with a low-temperature-grown buffer layer was used for wetting the GaAs substrate. However, it is difficult to completely suppress the thermal decomposition of the substrate surface at growth temperature higher than 900°C, because the buffer layer itself is very thin (~ 20 nm) and is not homogeneous. As shown in Fig. 4.13 (a), the formation of mixed cubic/hexagonal structures in c-GaN layer grown at 960°C exhibited mixed ED patterns, which consist of different types of diffraction patterns related to the cubic (open circles) and hexagonal (open parallelogram and open triangles) structures. It is clearly seen in the Fig. 4.13 that the c-GaN $\{111\}$ and h-GaN (0002) diffraction spots are

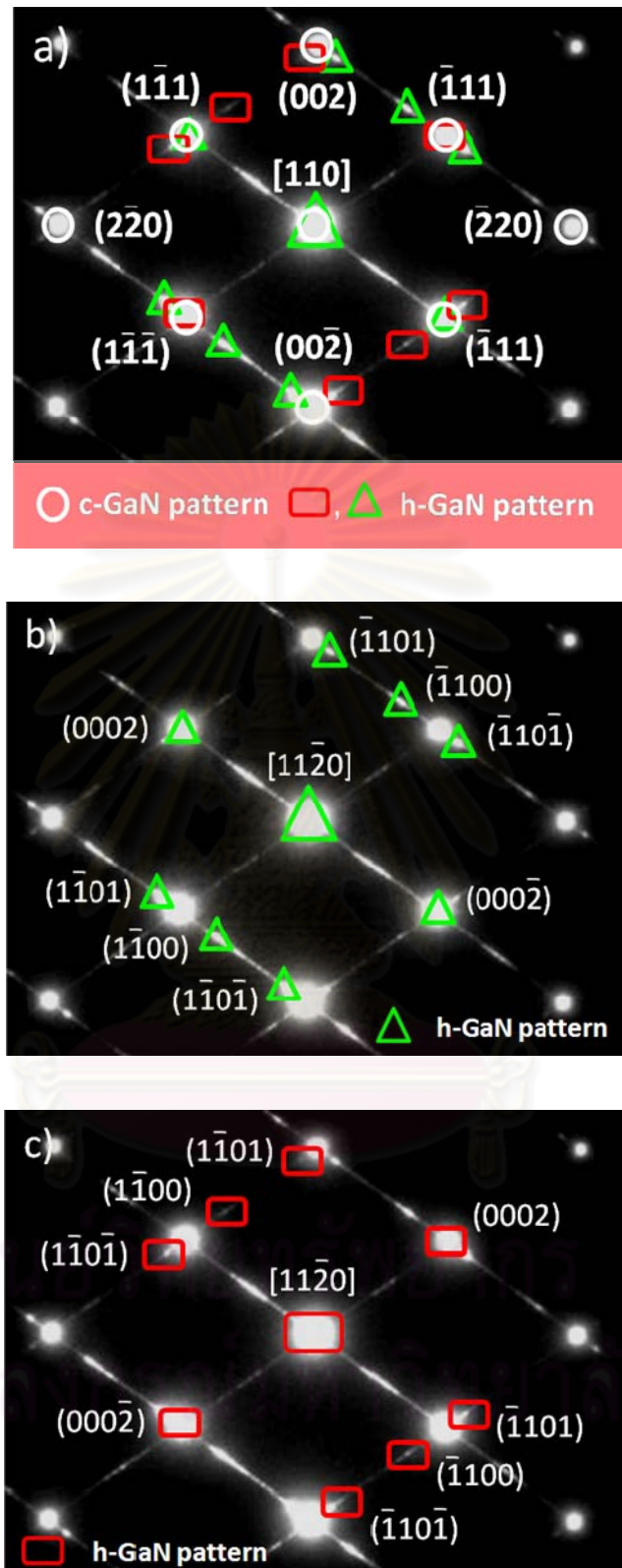


Figure 4.13: (a) ED pattern of c-GaN layer grown at 960°C showing mixed cubic/hexagonal structure. The key-diagrams show diffraction patterns for hexagonal structures orientated along (b) [1-11] (open triangles) and (c) [-111] directions indicated as the open triangles parallelograms, respectively.

overlapped. The implications of our observation are as followings. Along [110] zone axis, there are hexagonal sub-domains with different crystal orientations; $(1-11)_{c\text{-GaN}} // (0002)_{h\text{-GaN}}$ and $(-111)_{c\text{-GaN}} // (0002)_{h\text{-GaN}}$. Thus, an in-plane epitaxial relationship between hexagonal phase single crystal and c-GaN is $[110]_{c\text{-GaN}} // [11-20]_{h\text{-GaN}}$. Indeed, the crystal orientation of h-GaN is grow up along both the [1-11] (Fig. 4.13 (b)) and [-111] (Fig. 4.13 (c)) directions. In the above discussion, thermal decomposition of As atoms from the GaAs (001) surface is believed to be a key factor in the formation of {111} facets. Due to metastability of the c-GaN crystal, the hexagonal phase is often unexpectedly constructed on {111} facets in the cubic layer. This is due to the fundamental difference between cubic and hexagonal structures, which is rotated 60° about the cubic $\langle 111 \rangle$ and hexagonal $\langle 0001 \rangle$ axes. Thus, the cubic {111} planes can accommodate the growth of hexagonal structure along the $\langle 0001 \rangle$ directions.

4.6 Summary

The c-GaN layers grown on GaAs (001) substrates at various growth temperatures (900-960°C) and various growth temperature of GaN buffer layer (550-600°C) were investigated by cross-sectional TEM micrographs, ED patterns and DF technique to analyze effects of growth temperature on micro-structures. At the lowest temperature (900°C) and at the growth temperature of buffer layer at 575°C, there is less stacking faults and less intensity of the streak lines connecting the {111} reciprocal points to the (002) and (220) diffraction spots in the ED pattern. There is no diffraction spots related to hexagonal structure was observed; only cubic single diffraction spots are seen. With increasing growth temperature to 930-960°C and the growth temperature of buffer layer at 550 and 600°C, the single diffraction spots related to hexagonal structure were clearly observed in the ED pattern. Our results demonstrated that a region contained the high density of SFs can be accommodated to become seeds of hexagonal phase inclusions. Using ED patterns in TEM, the epitaxial relationship between layer and hexagonal phase sub-domains was determined to be $(111)_{c\text{-GaN}} // (0001)_{h\text{-GaN}}$ and $(110)_{c\text{-GaN}} // (11-20)_{h\text{-GaN}}$.

CHAPTER V

Microstructural Characterization of c-GaN on GaAs (311)

5.1 Sample Structure and Growth Conditions

According to the results and discussion of c-GaN films grown on GaAs (001) substrates, we found that the optimum temperature to grow cubic GaN phase is the growth temperature of c-GaN films layer 900°C and the growth temperature of LT-GaN buffer layer 575°C and Sanorpim *et al.* reported a reduction of SFs and twins which is likely resulted from their annihilation and termination within the c-GaN crystal due to the dominance of the lateral growth of the stable (311)A facets. This motivates us to investigate the structural characteristics of c-GaN grown on GaAs (311) substrate with growth temperature of c-GaN films layer 900°C and growth temperature of LT-GaN buffer layer 575°C as shown in Fig. 5.1.

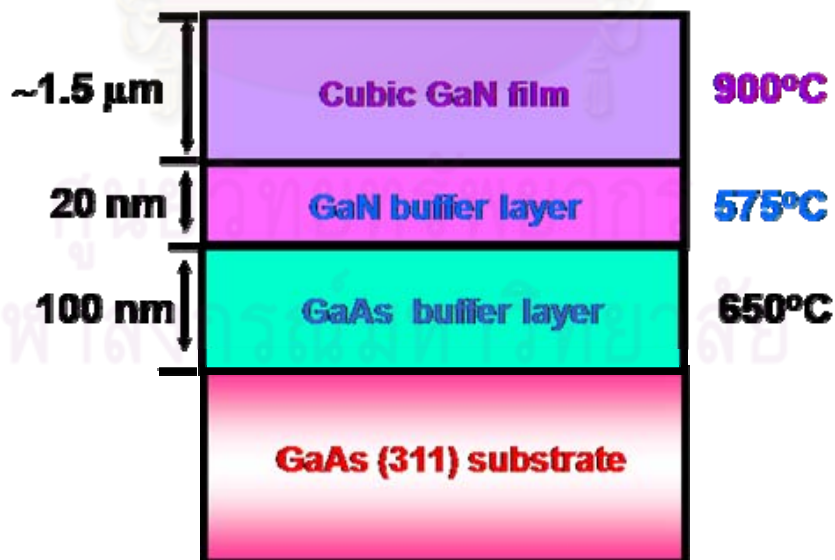


Figure 5.1: Schematic drawing of c-GaN sample grown on GaAs (311) substrate with growth temperature of c-GaN films layer 900°C and growth temperatures of LT-GaN buffer 575°C.

5.2 Morphologies of Surface and Interface

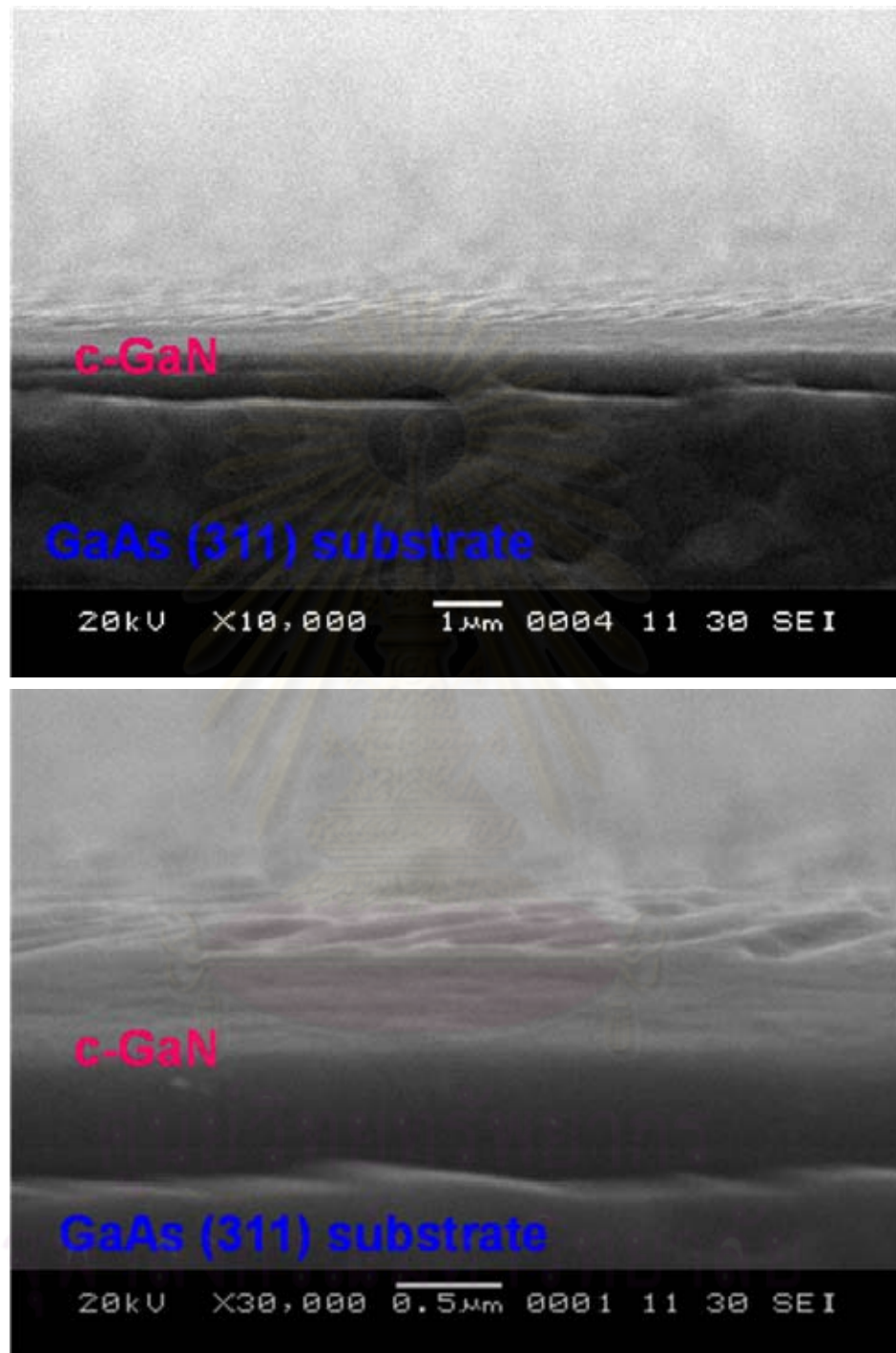


Figure 5.2: SEM images showing cross-section and surface of the c-GaN films grown on GaAs (311) substrate with growth temperature of c-GaN films layer 900°C and growth temperature of LT-GaN buffer layer 575°C

Figure 5.2 shows SEM images illustrating cross-section and surface of the c-GaN films grown on the GaAs (311) oriented substrates. Obviously, both the surface of c-GaN films layer and the GaN buffer layer are smoother than both surfaces of c-GaN films grown on GaAs (001) substrates. As the discussion in topic 4.2, the deposition of high-temperature ($\sim 900^\circ\text{C}$) of c-GaN films layer and the low sublimation point of As are causing the As thermal decomposition which bring to the generation of (111) step on the GaAs (001) grown layer. In which the GaAs (311) grown surface is used as the substrate, it is difficulty of the generation of the (111) step on the GaAs (311) grown surface. There is no voids at the GaN/GaAs interface and any defects are invisible. In macroscopic, it seems to be the c-GaN grown on GaAs (311) substrate is higher quality than the c-GaN grown on GaAs (001) substrates. Thus, the TEM analysis was used to investigate the structural characteristics and the extended defects.

Plan-view TEM micrographs and ED pattern (in Fig. 5.3) are representing the surface of c-GaN films related to the formation of planar defects and dislocations. The plan-view TEM micrograph as shown in Fig. 5.3 (a) is noticed there are threading dislocations appearing on the GaN surface. For Fig. 5.3 (b) the occurrence of stacking faults (SFs) is observed and the dislocations (DTs) are still remaining relating to the ED pattern. These defects are diffracting and showing in form of the bigger spots such as the diffracting spots from (02-2) and (0-22) planes.

ศูนย์วิทยทรัพยากร
จุฬาลงกรณ์มหาวิทยาลัย

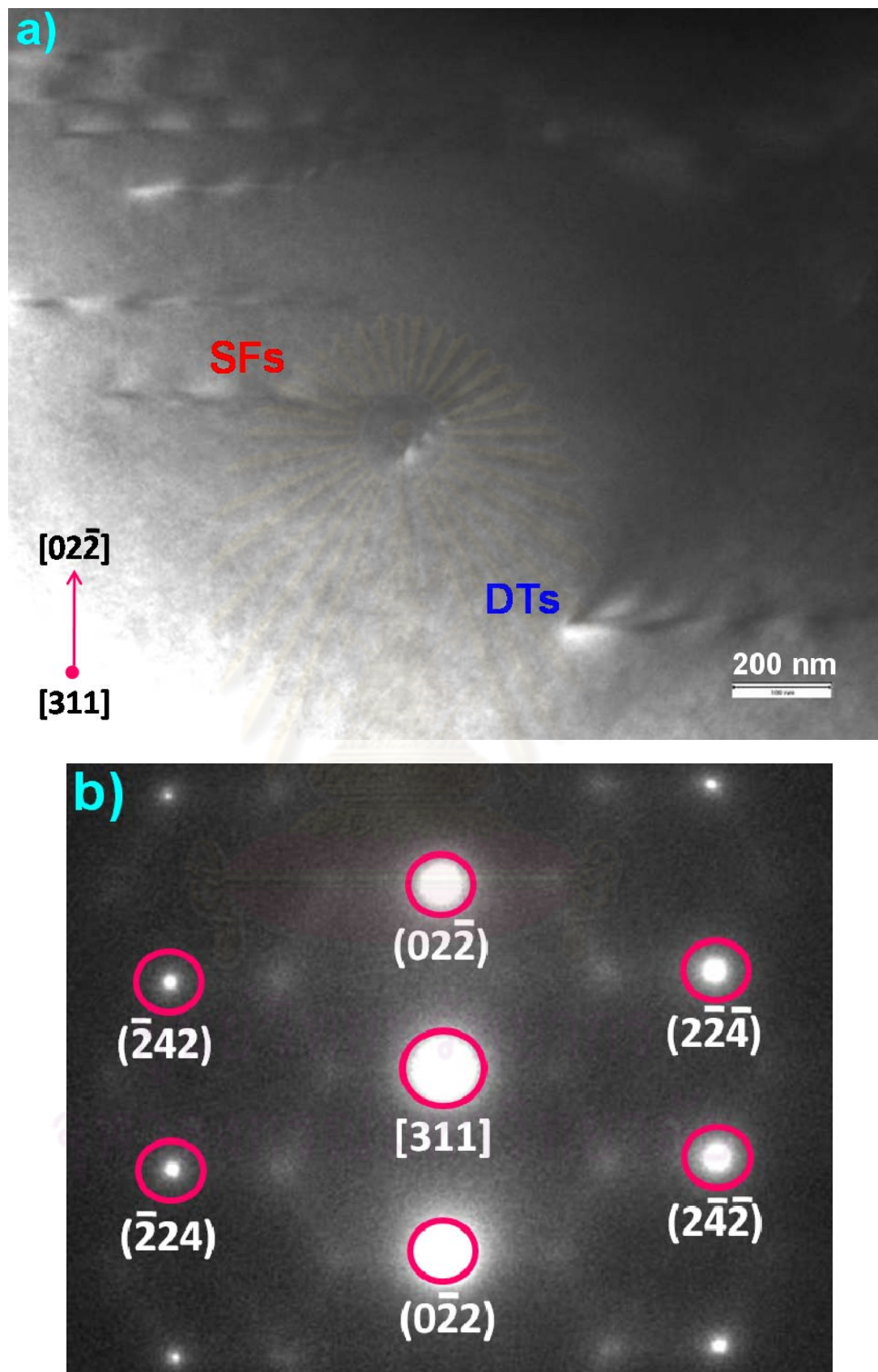


Figure 5.3: Showing plan-view micrographs and ED pattern of the c-GaN films grown on GaAs (311) substrate.

5.3 Microstructures in c-GaN on GaAs (311)

The specimen; c-GaN grown on GaAs (311) substrate with growth temperature of films layer 900°C and growth temperature of LT-GaN buffer layer 575°C was prepared by the cross-sectional TEM preparation process and characterized by TEM analysis as follows:

Figure 5.4 presents a cross-sectional TEM micrograph and ED pattern of c-GaN films grown at 900°C and GaN buffer layer grown at 575°C on GaAs (311) substrate. From the cross-sectional TEM micrograph (Fig. 5.4 (a)) we found that the existence of SFs lying on the (111) facets with an angle of 29.5° inclined from the (311) substrate surface. Moreover, the GaN surface is noticeable decomposed corresponding to the metastability of cubic GaN phase and these lines are observed and distributed on the c-GaN films layer. The amount and distribution of such defects seriously affects on the crystalline quality since the occurrence of the (111) lines is probably breaking into the (111) planes decomposition. However, we observed that there is a weak streak connecting the {111} spots to the (-112) spot and there is no different type of single diffraction spot so the GaN films has the cubic structure without the hexagonal inclusions.

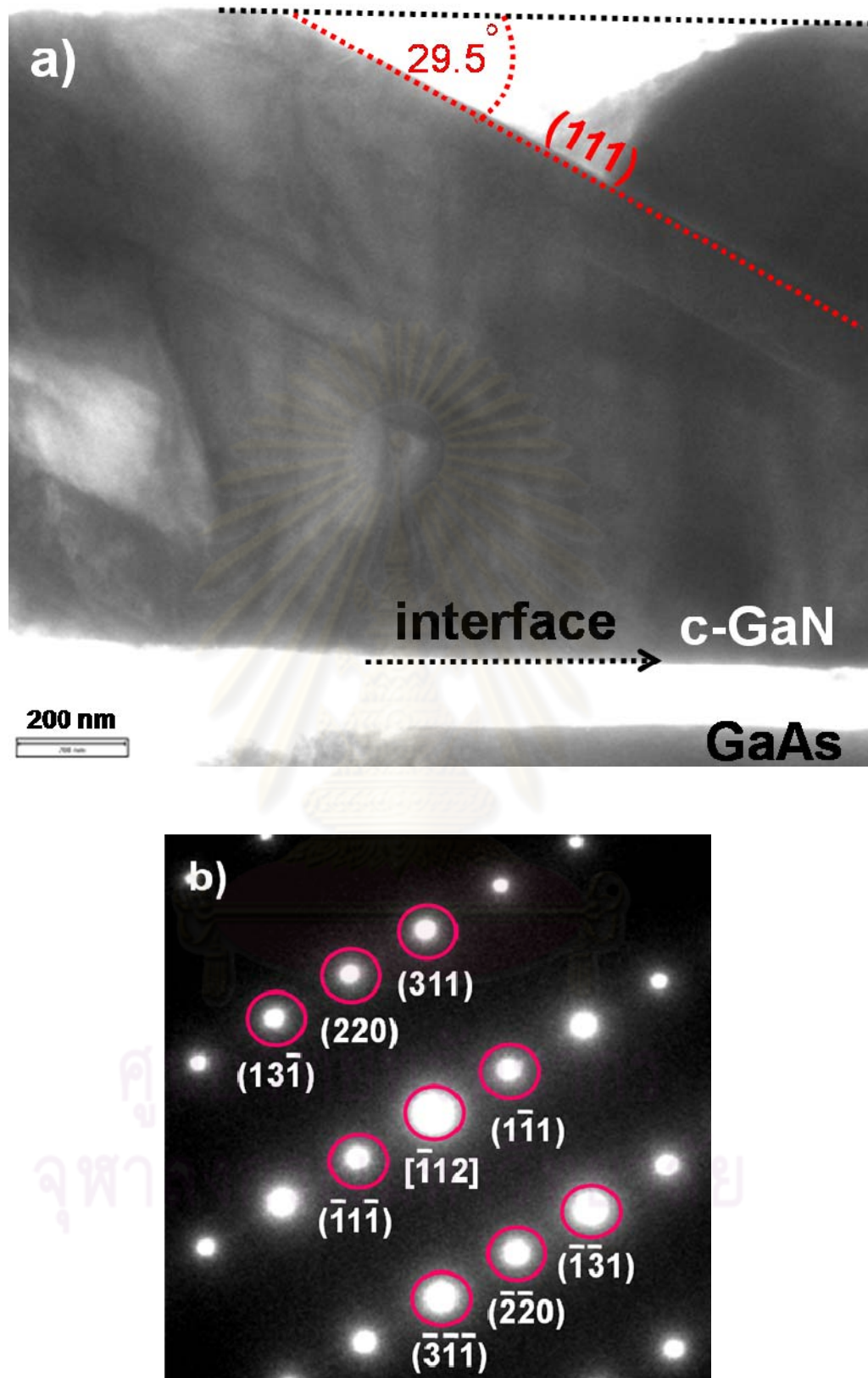


Figure 5.4: Cross-sectional TEM micrograph and ED pattern of c-GaN layers grown on GaAs (311) substrates with growth temperature of GaN films layer 900°C and growth temperature of LT-GaN buffer layer 575°C .

5.4 SFs in c-GaN on GaAs (311)

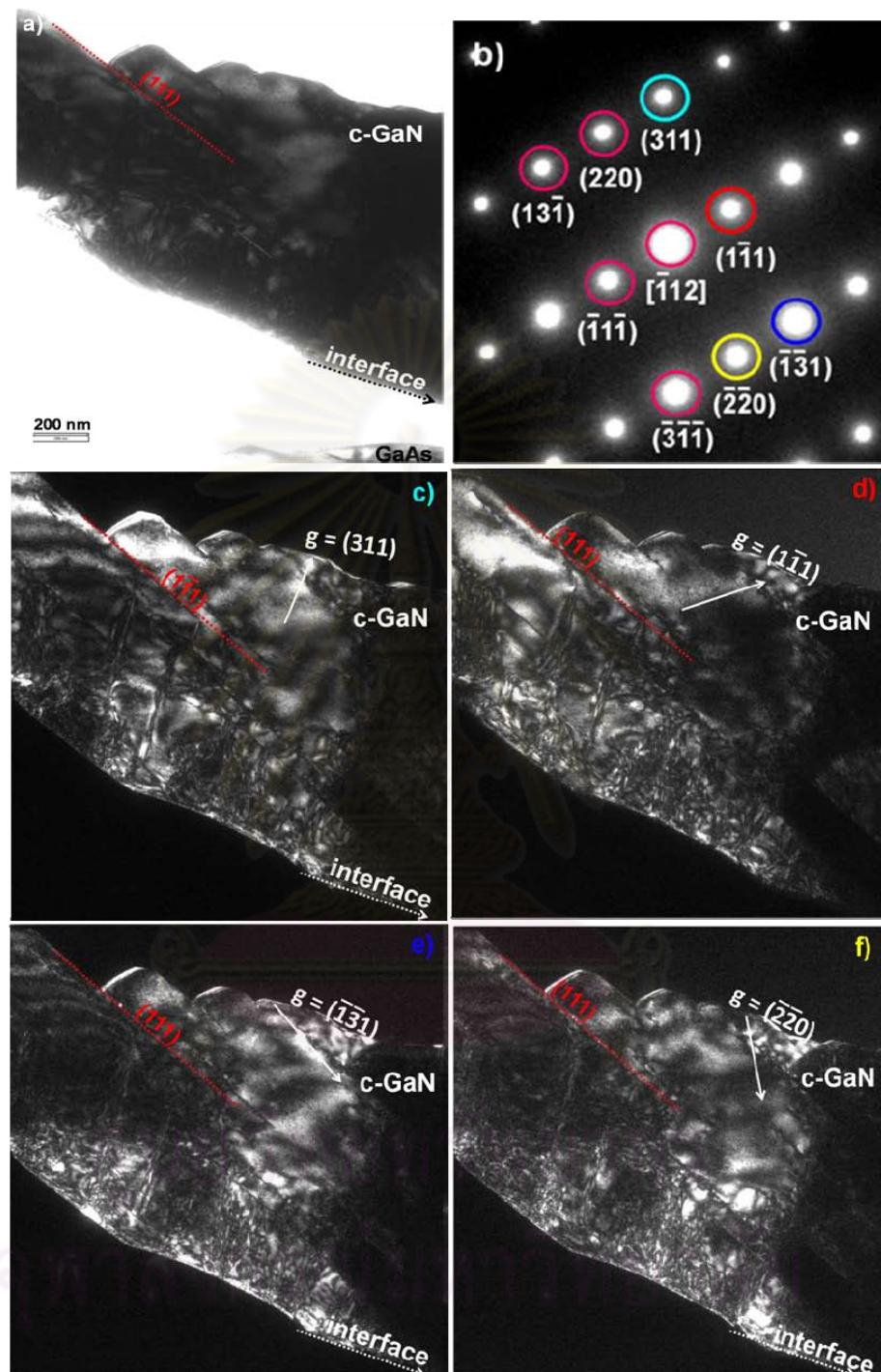


Figure 5.5: Cross-sectional TEM (a) micrograph and (b) ED pattern of c-GaN films layer grown on GaAs (311) substrates with growth temperature of films layer 900°C and growth temperature of GaN buffer layer 575°C. Dark-field (DF) images of the diffracted spots taken from (c) (311), (d) (1-11), (e) (-1-31) and (f) (-2-20)

Figure 5.5 shows a cross-sectional TEM micrograph in Fig. 5.5 (a) bright-field (BF) image, Fig. 5.5 (b) ED pattern of c-GaN films layer grown on (311) surface and dark-field (DF) images have taken in selected area diffraction as BF-TEM image from the diffraction spots of Figs. 5.5 (c) (311), (d) (1-11), (e) (-1-31) and (f) (-2-20). In order to verify the existence of the (111) lines distributed in c-GaN films layer, the (111) planes decomposition and the SFs, we are concentrating to the DF-TEM image from the (1-11) diffraction spot (in Fig. 5.5 (d)). The bright contrast region is demonstrating the (111) lines and the GaN surface at the decomposition region lying on (111) facets. Besides, the other spots such as (311), (-1-31) and (-2-20) are representing the diffracting planes as the bright contrast region which we follow up to investigate and predict the formation of planar defects.

5.5 Discussion

The c-GaN layers grown on GaAs (311) substrates at growth temperature of c-GaN films layer 900°C and growth temperature of LT-GaN buffer layer 575°C were investigated by SEM, plan-view TEM micrographs and ED pattern and cross-sectional TEM micrographs and ED patterns to analyze effects of substrate surface on micro-structures. There is no voids at the GaN/GaAs interface in which we found that the SFs generated from the (111) step on substrate surface. Although the thermal As decomposition is decomposing from the (311) oriented surface, it is difficult to form the (111) step surface. There is less SFs and less intensity of the streak lines connecting the {111} reciprocal points to the (-112) diffraction spot in the ED pattern. No diffraction spots related to hexagonal structure was observed; only cubic single diffraction spots are seen. Our results demonstrated that there is no a region contained the high density of SFs can be accommodated to become seeds of hexagonal phase inclusions. However, the GaN surface decomposition is demonstrated and affecting to the quality of cubic GaN films.

5.6 Summary

The c-GaN grown on GaAs (311) substrate with growth temperature of c-GaN films layer of 900°C and growth temperature of LT-GaN buffer layer of 575°C was investigated by cross-sectional TEM micrographs, ED patterns and DF technique to investigate the microstructural characterization of c-GaN on GaAs (311) substrate and assess with the microstructural characterization of c-GaN (001) substrate. The results from c-GaN grown on GaAs (311) substrate represent there is no voids, less SFs, less the intensity of streaking connecting to the diffraction spots and these results demonstrate the better quality of c-GaN grown on GaAs (311) substrate is more than c-GaN grown on GaAs (001) substrate with identical growth conditions.



CHAPTER VI

CONCLUSIONS

In the thesis, the author described a study of the structural characterization of the c-GaN (001) and (311) films grown on GaAs (001) and (311) substrate by MOVPE. Transmission electron microscopy(TEM) were mainly used to investigate the structural modification, crystal quality and structural defects of the c-GaN films including the c-GaN (001) and (311) films grown on GaAs (001) and (311) substrates, respectively. The discussion was focused on the different of growth conditions, especially the various growth temperature of c-GaN films layer and various growth temperature of LT-GaN buffer layer of the c-GaN (001) films on GaAs (001) substrates and the c-GaN (311) films on GaAs (311) substrate. The main results and conclusions obtained in this research work are summarized as follows:

(1) The lowest temperature (900°C) of c-GaN (001) films has a cubic structure with no stacking faults (SFs), hexagonal inclusions and the streaking lines connecting the {111} reciprocal points to the (002) and (220) diffraction spots in the ED pattern even at the GaN/GaAs interface .

(2) The 575°C growth temperature of GaN buffer layer with 900°C growth temperature of c-GaN (001) films layer has the highest cubic phase purity and less of planar defects.

(3) The c-GaN (311) films grown on GaAs (311) substrate with growth temperature of c-GaN (311) films layer at 900°C and growth temperature of GaN buffer layer at 575°C has a cubic structure with less SFs, less weak streaking lines in ED pattern and no any voids at the GaN/GaAs interface.

REFERENCES

- [1] Dapeng, X., et al. Investigation on quality of cubic GaN/GaAs (100) by double-crystal X-ray diffraction. Journal of Science in China (Series A) 42 (1999): 517-522.
- [2] Vennegues, P., Beaumont, B., Bousquet, V., Vaille, M., and Gibart, P. Reduction mechanisms for defect densities in GaN using one- or two- step epitaxial lateral overgrowth method. Journal of Applied Physics 87 (2000): 4175-4181.
- [3] Sakai, A., Sunakawa, H., and Usui, A. Defect structure in selectively grown GaN films with low threading dislocation density. Journal of Appl. Phys. Lett. 71 (1997): 2259-2261.
- [4] Nakadaira, A., and Tanaka, H. Growth of Zinc-Blende GaN on GaAs (100) substrates at high temperature using low-pressure MOVPE with low V/III molar ratio. Journal of Electronic Materials 26 (1997): 320-324.
- [5] Maksimov, O., et al. Structural and optical properties of GaN films grown on GaAs substrates by molecular beam epitaxy. Journal of Vacuum 80 (2006): 1042-1045.
- [6] Akasaki, I. Nitride semiconductors – impact on the future world. Journal of Crystal Growth 237-239 (2002): 905-911.
- [7] Sanorpim, S., Katayama, R., Yoodee, K., and Onabe, K. Growth mechanism and structural characterization of hexagonal GaN films grown on cubic GaN (111)/GaAs (111)B substrates by MOVPE. Journal of Crystal Growth 275 (2005): e1023-e1027.
- [8] Wu, J., Yaguchi, H., Onabe, K., Ito, R., and Shiraki, Y. Optical transitions in cubic GaN grown on GaAs (100) substrates by metalorganic vapor phase epitaxy, Journal of Crystal Growth 189/190 (1998): 415-419.
- [9] Okumura, H. et al. Growth and characterization of cubic GaN, Journal of Crystal Growth 178 (1997): 113-133.
- [10] Wu, J., Zhao, F., Onabe, K., and Shiraki, Y. Metalorganic vapor-phase epitaxy of cubic GaN on GaAs (100) substrates by inserting an intermediate protection layer. Journal of Crystal Growth 221 (2000): 276-279.
- [11] Onuma, T., Nozaka, T., Yamaguchi, H., Suzuki, T., and Chichibu, S.F. Cross-sectional spatially resolved cathodoluminescence study of cubic GaN films grown by metalorganic vapor phase epitaxy on free standing (001) 3C-SiC and GaAs substrates. Journal of Crystal Growth 298 (2007): 193-197.

- [12] Wu, J., Yaguchi, H., Onabe, K., Ito, R., and Shiraki, Y. Photoluminescence properties of cubic GaN grown on GaAs (100) substrates by metalorganic vapor phase epitaxy. Journal of Appl. Phys. Lett. 71 (1997): 2067-2069.
- [13] Tachibana, H. et al. Relation between GaAs surface morphology and incorporation of hexagonal GaN into cubic GaN. Journal of Crystal Growth 196 (1999): 41-46.
- [14] Bo, Q. et al. Surface roughness and high density of cubic twins and hexagonal inclusions in cubic GaN epilayers. Journal of Science in China (Series A) 44 (2001): 796-800.
- [15] Kangawa, Y., Akiyama, T., Ito, T., Shiraishi, K., and Kakimoto, K. Theoretical approach to structural stability of c-GaN: How to grow cubic GaN. Journal of Crystal Growth 311 (2009): 3106-3109.
- [16] Huang, S. et al. Growth of wurtzite GaN on (001) GaAs substrates at low temperature by atomic layer epitaxy. Journal of Materials Science Letters 17 (1998): 1281-1285.
- [17] Xu, D. et al. Gallium diffusion through cubic GaN films grown on GaAs (100) at high-temperature using low-pressure MOVPE. Journal of Crystal Growth 191 (1998): 646-650.
- [18] Tricker, D.M., Brown, P.D., Cheng, T.S., Foxon, C.T., and Humphreys, C.J. A TEM study of substrate pitting during the MBE growth of GaN on GaAs and GaP substrates. Journal of Applied Surface Science 123/124 (1995) 22-27.
- [19] A.G. Bhuiyan, A. Hashimoto, A. Yamamoto and R. Ishigami. Nitridation effects of GaP (111)B substrate on MOCVD growth of InN. Journal of Crystal Growth 212 (2000): 379-384.
- [20] Wu, D., Lin, W., Pan, C., and Horng, R. Growth characteristics of GaN on (001) GaP substrates by MOVPE. Journal of Crystal Growth 221 (2000):286-292.
- [21] Chang, M.N., Hsieh, K.C., Nee, T.-E., Chuo, C.C., and Chyi, J.I. Behavior of arsenic precipitation in low-temperature grown III-V arsenides. Journal of Crystal Growth 201/202 (1999): 212-216.
- [22] Ott, A.K., Casey, S.M., and Leone, S.R. Arsenic desorption kinetics from Si (100). Journal of Surface Science 405 (1998): 228-237.
- [23] Sanorpim, S., Takuma, E., Onabe, K., Ichinose, H., and Shiraki, Y. Laterally overgrown GaN on patterned GaAs (001) substrates by MOVPE. Journal of Phys. Stat. Sol. (a) 192 (2002): 446-452.

- [24] Sanorpim, S. et al. Reduction of planar defect density in laterally overgrown cubic-GaN on patterned GaAs (001) substrates by MOVPE. Journal of Phys. Stat. Sol. (b) 234 (2002): 840-844.
- [25] Fultz, B., and Howe, J. Transmission electron microscopy and diffractometry of materials. 2nd Edition. Springer, 2002.
- [26] Williams, D.B., and Carter, C.B. Transmission Electron Microscopy, A textbook for Materials Science. New York, USA: A Division of Plenum Press Publishing Corporation, 1996.
- [27] Edington, J.W. Practical electron microscopy in materials science. Van Nostrand Reinhold Company, 1976.
- [28] Suandon, S. Structural property analysis of GaN grown on GaAs by MOVPE using transmission electron microscopy. Master's Thesis, Department of Physics Faculty of Science Chulalongkorn University, 2005.
- [29] Liu, L., and Edgar, J.H. Substrates for gallium nitride epitaxy. Materials Science and Engineering R 37 (2002) 61.
- [30] Jung, H. D., and Kumagai, N. Optical anisotropy and Surface morphology of InGaAs lattice-mismatched with GaAs (001). Journal of Appl. Phys. 84 (1998): 5497.
- [31] Trampert, A., Brandt, O., Yang, H., and Ploog, K. H. Growth of cubic GaN on Si(001) by plasma-assisted MBE. Journal of Appl. Phys. Lett. 70 (1997): 583.
- [32] Brandt, O., Yang, H., Trampert, A., Wassermeier, M., and Ploog, K. H. Ga-terminated β -GaN(001) surface reconstructions studied by scanning tunneling microscopy. Journal of Appl. Phys. Lett. 71 (1997): 473.



APPENDICES

ศูนย์วิทยทรัพยากร
จุฬาลงกรณ์มหาวิทยาลัย

APPENDIX A

CONFERENCE PRESENTATIONS

- [1] **Surang Sumnavadee**, Sakuntam Sanorpim and Kentaro Onabe. Observation of Hexagonal Phase Generation in Cubic-Phase GaN grown by Metal-organic Vapor Phase Epitaxy with Different Growth Temperatures of buffer layer, *the 4th Siam Physics Congress (SPC 2009): Physics for Dynamic Society, Petchaburi, Thailand (2009)* (Poster).
- [2] **Surang Sumnavadee**, Sakuntam Sanorpim and Kentaro Onabe. TEM Analysis of Growth Temperature Effect on Hexagonal Phase Generation in Cubic-Phase GaN layer on GaAs (001) Substrate, *the 35th Congress on Science and Technology of Thailand (STT 35), Chonburi, Thailand (2009)* (Oral).
- [3] **Surang Sumnavadee**, Sakuntam Sanorpim and Kentaro Onabe. Microstructures in Cubic-Phase GaN/GaAs (001) Grown by Metalorganic Vapor Phase Epitaxy, *the 7th Eco-Energy and Materials Science and Engineering Symposium (EMSES 2009), Chaingmai, Thailand (2009)* (Oral).
- [4] **Surang Sumnavadee**, Sakuntam Sanorpim and Kentaro Onabe. Stacking Fault and Its Effect on c-GaN Epitaxial Growth on GaAs (001), *the 27th Microscopy Society of Thailand (MST 27), Suratthani, Thailand (2010)* (Oral).
- [5] **Surang Sumnavadee**, Sakuntam Sanorpim and Kentaro Onabe. Effect of growth temperature of buffer layer on c-GaN epilayer grow on GaAs(001) substrate, *the 5th Siam Physics Congress (SPC 2010): Physics for Creative Society, Kanjanaburi, Thailand (2010)* (Oral).
- [6] **Surang Sumnavadee**, Sakuntam Sanorpim and Kentaro Onabe. Observation of strain and hexagonal phase generation in MOVPE growth of cubic GaN on GaAs (001) with different growth temperatures of GaN buffer layer, *the 14th International Summer School on Crystal Growth (ISSCG-14), Dalian, China (2010)* (Poster) (The best poster award).
- [7] **Surang Sumnavadee**, Sakuntam Sanorpim and Kentaro Onabe. Observation of strain and hexagonal phase generation in MOVPE growth of cubic GaN on GaAs (001) with different growth temperatures of GaN buffer layer, *the 16th International Conference of Crystal Growth (ICCG-16), Beijing, China (2010)* (Oral).
- [8] **Surang Sumnavadee**, Sakuntam Sanorpim and Kentaro Onabe. On the formation of stacking fault and dislocation in MOVPE growth of cubic GaN on GaAs (001): Effect of the growth temperature of cubic GaN buffer layer, *the 6th Siam Physics Congress (SPC 2011): Physics for all, all for physics, Chonburi, Thailand (2011)* (Poster).

APPENDIX B

Publication

[1] Sumnavadee, S., Sanorpim, S., Paosawat, B., and Onabe, K. Stacking fault and its effect on c-GaN epitaxial growth on GaAs (001). Journal of the Microscopy Society of Thailand. 24 (2010): 136-139.



ศูนย์วิทยทรัพยากร
จุฬาลงกรณ์มหาวิทยาลัย

APPENDIX C

The Best Poster Award



VITAE

Miss Surang Sumnavadee was born on July 7, 1983 in Bangkok, Thailand. She had received her bachelor degree of Education (Physics) from the Department of Education, Faculty of Science Teaching (Physics), Kasetsart University in 2004, and continued her Master's study at Chulalongkorn University in 2007.

One of her papers has been accepted to be published in Journal of the Microscopy Society of Thailand 24(2), 136-139 (APPENDIX B). The other has been published in the proceeding of 7th Eco-Energy and Materials Science and Engineering Symposium, Thailand. One of her posters has been awarded the best poster award in an international conference; ISSCG-14 (APPENDIX C). She has also participated in oral and poster presentations (APPENDIX A).



ศูนย์วิทยทรัพยากร
จุฬาลงกรณ์มหาวิทยาลัย